H204

A Calorimetric Measurement of Decay Heat From ^{235}U Fission Products From 10 to 10^5 Seconds

EPRI

EPRI NP-616
Project 230
Final Report
Volume 1
February 1978

aj.2

Keywords:
Decay Heat
Fossil Product After Heat

Prepared by
University of California
Berkeley, California

A Calorimetric Measurement of Decay Heat From ^{235}U Fission Products From 10 to 10^5 Seconds

NP-616, Volume 1
Research Project 230

Final Report, February 1978

Prepared by

UNIVERSITY OF CALIFORNIA
Berkeley, California 94720

Principal Investigators
V. E. Schrock
L. M. Grossman
S. G. Prussin
K. C. Sockalingam
F. Nuh
C-K Fan
N. Z. Cho
S. J. Oh

Prepared for

Electric Power Research Institute
3412 Hillview Avenue
Palo Alto, California 94304

EPRI Project Manager
Frank J. Rahn
Nuclear Power Division

FOREWORD

The recoverable energy release rate, commonly referred to as decay heat, from the decay of radioactive fission products is of great importance in the safety analysis of power reactors. Until recently the accuracy with which this time dependent quantity could be specified was lower than required for evaluation of safety margins. The American Nuclear Society Draft Standard ANS 5.1 adopted the uranium fuel decay heat curve for "infinite irradiation" proposed by K. Shure but estimated the uncertainty to be +20%, -40% for the first 10^3 seconds after shutdown and +10%, -20% between 10^3 and 10^7 seconds after shutdown. The Atomic Energy Commission utilized the ANS Draft Standard in various ways in the regulatory process. The most important is the specification in the Code of Federal Regulations that Loss-of-Coolant Accident (LOCA) analysis shall use ANS 5.1 plus 20% for the fission product decay heat. This requirement has been viewed widely as excessively conservative and has prompted new research aimed at improved accuracy of our knowledge of decay heat.

The Electric Power Research Institute (EPRI) has sponsored research into the decay heat of ^{235}U at the University of California, Berkeley. Volume I of this report gives the results of an experimental calorimetric measurement of the absorbed radiation versus time from fission product decay. Volume II presents the results of research on the summation calculation method. In addition to the work reported herein, EPRI has also sponsored related work at IRT Corporation on the measurement of the decay heat of ^{235}U and ^{239}Pu under contracts RP392, 766-1, and 957-1. The data obtained from these projects, along with other experimental and analytical data from projects sponsored by the NRC, has led to a new ANS 5.1 Draft Standard with much lower estimated uncertainties. This new Draft Standard will significantly contribute toward a more realistic analysis of a postulated Loss-of-Coolant Accident, leading to a better quantified estimate of the safety margins of Light Water Reactors.

Frank J. Rahn
Safety and Analysis Department
Nuclear Power Division

ABSTRACT

A calorimetric measurement of decay heat power of ^{235}U fission products has been made using a fast response calorimeter in the cooling time range from 10 to 10^5 seconds. The calorimeter is based on measurement of the rate of change of energy stored in a mercury absorber together with measurement of heat flow through a thermopile. Agreement between the measured values and summation calculations is good in the cooling time range from 500 to 10^4 seconds. At earlier times the accuracy potential of the instrument was not realized; the average of measured results is higher than predicted by up to 17%. The estimated uncertainty of the measurement is 3.4% (one sigma) from 400 to 10^4 seconds and rises to 22.7% at 11 seconds.

CONTENTS

Section		Page
1.	Introduction	1
2.	Description of the Calorimeter	10
	2.1 General	10
	2.2 Dilatometer	10
	2.3 Thermopile	16
	2.4 Fissile Samples	18
	2.5 Transfer System	20
	2.6 Predicted Response of the Calorimeter	22
	2.7 Instrumentation	23
	2.8 Calibration Procedure	25
3.	Irradiation Facility	29
4.	Experimental Procedure	30
	4.1 Procedures	30
	4.2 Test Conditions	31
5.	Measurement of Number of Fissions in Samples	33
6.	Decay Heat Results	53
	6.1 Data Reduction Procedure	53
	6.2 Decay Heat Results	55
	6.3 Error Assessment	68
	6.4 Comparison of Results with other Experiments and Summation Calculations	74
7.	Conclusions	75
8.	References	76

List of Figures

Page

1. Schematic of the Calorimeter 11
2. Sample Tube Details 12
3. Schematic of the Dilatometer 15
4. Thermopile 17
5. Fissile Sample 19
6. Transfer System 21
7. Theoretical Response to Decay Heat 24
8. Theoretical Response to Step Electric Power Input 27
9. Actual Response to Step Input 27
10. Variation in Neutron Flux, 22.3 Hour Irradiation 35
11. Variation in Neutron Flux, 1 Hour and 4 Hour Irradiations 36
12. Fission Assay Counting System 37
13. Raw Data Run 1 56
14. Raw Data Run 8 57
15. Decay Heat Results for 1 Hour Irradiation 58
16. Decay Heat Results for 4 Hour Irradiation 59
17. Decay Heat Results for 22.35 Hour Irradiation 60
18. Comparison of UCB Results with others on Infinite Irradiation Basis 69
19. Comparison of UCB with IRT Data for Nominal 1 Day Irradiation 73

SUMMARY

The research reported here was conducted with the objective of obtaining accurate experimental information on the energy release rates from the decay of fission products in nuclear fuel, with particular emphasis on short times after shutdown. In this research program a calorimetric approach was chosen. Another EPRI research program at IRT Corporation, San Diego, California, has utilized a radiation detection experimental method (see EPRI Report NP-180).

Early attempts at calorimetric measurements of fission product decay heat have been limited to shutdown times greater than about 100 seconds; this limitation arising from the inherently long time constant that is associated with the massive absorber needed to absorb the gamma rays. The calorimeter used in the present research was designed to give fast response to the absorbed gamma energy. The beta energy is transferred to the mercury with a time constant less than one second, achieved by careful heat transfer design, and is promptly measured by the mercury dilation. The delayed transfer of energy from the mercury absorber to the thermostatic block is measured by an interconnecting thermopile.

Measurements were made of the decay heat from uranium samples irradiated at a neutron flux of approximately 10^{14} neutrons/sec-cm^2 for periods of 1, 4, and 22.3 hours. The measurements were made at shutdown times starting at 11 seconds and extending to 10^5 seconds. A total of seven runs are reported.

A thermally induced strain of the mercury container required a correction procedure that resulted in a reduction in accuracy of the results, particularly during the first 100 seconds, and the results in the early time are systemmatically higher than those measured in other recent research programs and those calculated by the summation method using the best nuclear data file.

The data for the three irradiation times used were put on the common basis of infinite irradiation and the uncertainty estimated. The mean value is higher than the summation calculation result by 12% at a shutdown time of 11 seconds. The difference rises to 17% at 40 seconds and then drops to values within about 1% for times between 500 and 10^4 seconds. The uncertainty (one sigma) is 22.7% at 11 seconds and drops to 3.4% at 400 seconds and remains constant at this value until 10^4 seconds. For longer shutdown times the uncertainty rises rather sharply owing to the small magnitude of the decay heat.

The calorimetric concept developed in this research program appears to be potentially capable of very accurate measurements of decay heat at cooling times as short as 10 seconds. The full potential was not realized in the present measurements because the mercury vessel rigidity was inadequate. This problem does not seem insurmountable in future designs.

1. Introduction

1.1 General

The recoverable energy release rate, commonly referred to as decay heat, from the decay of radioactive fission products is of great importance in the safety analysis of power reactors. Until recently the accuracy with which this time dependent quantity could be specified was lower than required for evaluation of safety margins. The American Nuclear Society Draft Standard ANS 5.1[1] adopted the uranium fuel decay heat curve for "infinite irradiation" proposed by K. Shure[2] but estimated the uncertainty to be +20%, -40% for the first 10^3 seconds after shutdown and +10%, -20% between 10^3 and 10^7 seconds after shutdown. The Atomic Energy Commission utilized the ANS Draft Standard in various ways in the regulatory process. The most important is the specification in the Code of Federal Regulations [3] that Loss-of-Coolant Accident (LOCA) analysis shall use ANS 5.1 plus 20% for the fission product decay heat. This requirement has been viewed widely as excessively conservative and has prompted new research aimed at improved accuracy of our knowledge of decay heat.

There are three methods for the determination of decay heat from fission products:

i) Measurement of the β and γ energies by spectroscopy. These results and their internal consistency have been discussed by K Shure[2], M. Lott[4] and Perry, et. al.[5]. More recent measurements of this type have been reported by J. K. Dickens et. al.[6] and S. J. Friesenhahn et. al.[7]. The older measurements suffered from a lack of internal consistency.

ii) Calorimetric measurement of the absorbed radiations from fission product decay. The earlier measurements of this type were reviewed by the same authors, (2) (4) and (5). The need for a massive absorber to capture the gamma rays generally leads to a long time constant of the apparatus making it unsuitable for short times after shutdown (short cooling time). This method will be reviewed in greater detail in the next section.

iii) Summation Calculations. This method consists of solving numerically the large

set of ordinary differential equations that describe the production and decay of each nuclide. The resulting time dependent inventory of nuclides and their decay properties are used to obtain individual contributions to decay heat and the results summed. Examples of computer codes for these calculations are: ORIGEN[8], CINDER[9], RIBD[10], PICFE[11], FISS[12] and COMBO[13]. The method is essentially exact but many of the required nuclear data are imprecisely known. Recent improvements in the Evaluated Nuclear Data File (ENDF -BIV) and statistical error assessments by Spinrad et. al.[14], Schmittroth[15] and Schmittroth and Schenter[16] have added confidence in the results obtained by this method but direct experimental verification is still needed.

1.2 Previous Calorimetric Measurements

a. Using a Calvet microcalorimeter, K. Johnston[17] measured the total energy emitted by the fission products of a sample of ^{239}Pu irradiated at Dounreay, U.K. The fuel sample was 40 mg. of powdered PuO_2 sealed in an aluminium capsule. The integrated flux was 1.89×10^{21} $n.cm^{-2}$ and no sample was irradiated continuously for more than nine days. Measurements were made for cooling times between forty and one hundred fifty days.

The microcalorimeter consisted of silver cells surrounded by multiple junction thermopiles and set in an aluminium block. Heat flow was compensated by Peltier cooling, reducing the temperature difference to zero, and γ absorption was accomplished through natural uranium surrounding the sample. Calibration was carried out by Joule heating. The number of fissions was determined by radiochemical analysis of ^{90}Sr, ^{95}Zr, and ^{144}Ce.

b. Calorimetric measurements of fast reactor fuel needles irradiated in RAPSODIE and FORTISSIMO were carried out by Devillers et. al.[18] in a twin microcalorimeter of conduction (Calvet-Tian) type. The copper cells were surrounded

by resistance elements forming the arms of a Wheatstone bridge and lodged in a thermostatic block of aluminium alloy. Heat transfer between the measurement and reference cells and the block was effected by Helium circulating at a low flow rate in a space of several millimeters between the cells and the thermostatic block. The time constant of the system was about 25 minutes. Calibration was by Joule heating.

The cooling times in the experiments were from 300 to 1600 days and the results were compared with summation calculations using PICPE with agreement around 1-4% after corrections to the experimental measurements for α activity of the trans-uranic elements, activation of the cladding, and γ leakage from the calorimeter. The experiment was designed to prove the possibility of calorimetric determination of burnup in fast reactor fuels.

c. Gunst, et. al.[19] measured in the MTR and ATR the decay heat of irradiated four rod assemblies of zircaloy clad oxide fuels of ^{235}U, ^{233}U, ^{239}Pu and ^{232}Th in a high flux ($\phi > 10^{14}$ n cm^{-2} sec^{-1}) using a simple underwater calorimeter of adiabatic type with heat leakage and stirrer corrections determined by calibration. Decay heat was measured as a function of cooling times from 14 hours to 4500 hours. Calculations were carried out using the 190 F.P. summation code COMBO; in general agreement between experiment and calculation was within 2%. For ^{235}U the experimental results (corrected for heavy isotopes, activation in the structure, and γ rays escaping from the calorimeter) agree with ANS 5.1 Proposed Standard (Shure curve) within a few percent.

d. The preceeding calorimetric experiments are for relatively large cooling times. In contrast, M. Lott, et. al.[20] have used a calorimetric method to obtain $E_\beta + E_\gamma$ for the thermal fissioning of ^{235}U for cooling times from 70 seconds to 1.5×10^7 sec. The microcalorimeter of conduction type is composed of twin cells, a measurement cell and a reference cell, which are thermally connected to a thermostatic block with identical thermopiles. The cells were made of silver 76 mm in diameter and 100 mm high. The two thermopiles were electrically connected in opposition

in order to cancel any signal arising from slight changes in the temperature of the thermostatically controlled block.

Sample capsules were made of a core of uranium (93% U^{235}) or plutonium (89% Pu^{239}) surrounded by a frame of zircaloy 2 with two thin (0.2 mm) foils of zircaloy 2 welded to the frame. The external dimensions of the cladding were 55 mm x 20 mm x 1.22 mm. The dimensions of the core were 45 mm x 16 x 0.80 mm. The weight of the fissile material was about 10 grams per sample. The calibration of the calorimeter was effected by Joule heating; the time constant about about 115 sec. The fission rate for irradiation in the natural U-graphite reactor ZOE was determined by gamma spectroscopy on ^{140}Ba. Gamma ray loss from the measurement cell was estimated by an eight group γ transport code. The difference between measured and calculated decay power was of the order of 10-12% (measured values higher than calculated) for cooling time <300 sec. and less than ±7% for cooling times >300 sec. The overall precision of measurement was ±5%.

In all of the preceding calorimeteric studies the treatment of the transient response of the calorimeter with a spatially distributed γ heat source in the absorbing volume is only approximately valid for long cooling times (quasi-static response) and may be seriously in error for short times <100 sec. The treatment of the calorimeter as a lumped parameter system, particularly the use of spatially concentrated electrical heating for calibration, introduces a systematic error which is significant in the early stages of the transient.

Very recently new approaches have been developed by Yarnell, et al[21], at LASL and in the EPRI sponsored project at the University of California, Berkeley reported herein. Yarnell used the principle of the isothermal boil-off calorimeter together with the extremely low specific heat of copper at the liquid helium temperature to achieve a time constant on the order of two seconds. The approach used in the present research combines the measurement of stored energy in a mercury absorber (by its dilatation) with a thermopile measurement of heat flow from the absorber to

a thermostat to achieve a time constant estimated to be less than one second.

1.3 Physical Principles of the UCB Calorimeter

It is not possible to measure heat generation directly, and all forms of calorimetery apply a version of the first law of thermodynamics to deduce the heat generation from a measurement of temperatures, temperature differences, phase changes, heat flows, etc. related to the heat source through the first law expression of the conservation of energy. In the case of large volume sources, the measurement of temperatures yields an inherently slow calorimeter due to the slowness of temperature equalization in a large volume.

The first law of thermodynamics can be written in general form for a continuous medium as

$$\dot{K} + \dot{E} = \oint_{\Sigma}(v_i\sigma_{ij} - q_j)n_j dA + \int_R(\rho v_i F_i + Q)d\tau \ .$$

Where $\dot{K}$ and $\dot{E}$ are the total kinetic energy and internal energy respectively of region R, bounded by a surface Σ with unit normal n_j, σ_{ij}, is the stress tensor, v_i the velocity components, q_j the heat flux vector, ρ the density, F_i the external force per unit mass, and Q the volumetric rate of heat generation.

From conservation of momentum,

$$\dot{K} = \oint_{\Sigma} v_i\sigma_{ij}n_j dA = \int_R \sigma_{ij} \frac{\partial v_i}{\partial x_j} d\tau + \int_R \rho v_i F_i d\tau$$

or

$$\int_R \left[\rho\frac{du}{dt} - \sigma_{ij}\frac{\partial v_i}{\partial x_j}\right] d\tau = -\oint_{\Sigma} q_j n_j dA + \int_R Q d\tau$$

where u is the internal energy per unit mass.

Since

$$\sigma_{ij} = -p\delta_{ij} + \tau_{ij}$$

and assuming the "dissipation function"

$$\Phi \equiv \int \tau_{ij} \frac{\partial v_i}{\partial x_j} d\tau$$

to be negligible in magnitude compared to other terms (in the following application), we have,

$$\int_R \left[\rho \frac{du}{dt} + p \frac{\partial v_j}{\partial x_j} \right] d\tau = -\oint_\Sigma q_j n_j dA + \int_R Q d\tau \ .$$

Using the continuity equation: $\frac{\partial v_j}{\partial x_j} = -\frac{1}{\rho} \frac{d\rho}{dt}$ and the definition of enthalpy,

$$h = u + p/\rho \quad ,$$

$$\int_R \left[\rho \frac{dh}{dt} - \frac{dp}{dt} \right] d\tau = -\oint_\Sigma \vec{q} \cdot \vec{n} \, dA + \int Q(\vec{r}, t) d\tau$$

From thermodynamic identities,

$$dh = \left(\frac{\partial h}{\partial T}\right)_p dT + \left[T\rho^{-2} \left(\frac{\partial \rho}{\partial T}\right)_p + \rho^{-1} \right]_T dp$$

$$\frac{dh}{dt} = C_p \frac{dT}{dt} + \left[T\rho^{-2} \left(\frac{\partial \rho}{\partial T}\right)_p + \rho^{-1} \right]_T \frac{dp}{dt}$$

and

$$\frac{dT}{dt} = \frac{\kappa}{\beta} \frac{dp}{dt} - \frac{1}{\rho\beta} \frac{d\rho}{dt}$$

where κ = "Isothermal compressibility" $\equiv \frac{1}{\rho}\left(\frac{\partial \rho}{\partial p}\right)_T$

β = "Coefficient of volume expansion" $\equiv -\frac{1}{\rho}\left(\frac{\partial \rho}{\partial T}\right)_P$

Substituting the two preceding equations in the integral energy balance yields,

$$\int_R \left[-\frac{C_p}{\beta}\frac{d\rho}{dt} + \left(\frac{\rho C_p \kappa}{\beta} - T\cdot\beta \right)\frac{dp}{dt} \right] d\tau = -\oint_\Sigma \vec{q}\cdot\vec{n}\, dA + \int_R Q(\vec{r},t)\, d\tau$$

Except for the neglect of the dissipation term, the above is an exact expression for a homogeneous region R with boundary surface Σ.

We now apply this energy balance to the following system. The portion A of the boundary is freely moving against a spring; the remainder of the boundary Σ-A is rigid and thermally conducting. The continuous medium in R contains a thermal source of power per unit volume $Q(\vec{r},t)$. The system is maintained nearly isothermal through the heat flux $\vec{q}$. The spatial variation in ρ and p are negligible. Under these conditions the volume integration on the L.H.S. of the preceding equation can be carried out as follows:

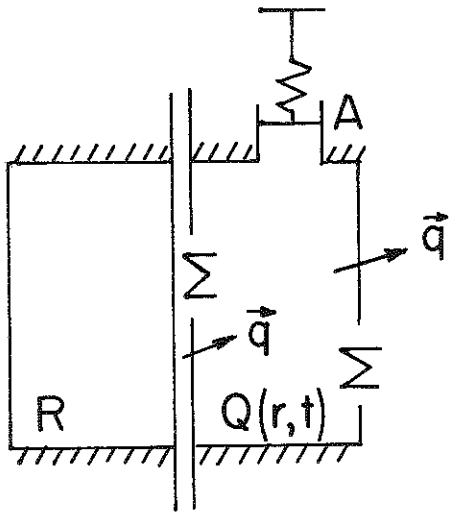

From continuity,

$$\int \frac{d\rho}{dt}\delta\tau = -\int \rho \frac{d}{dt}\delta\tau = -\rho\frac{d}{dt}\,\delta V$$

Also from the meaning of β,

$$\int T\beta\delta\tau = \delta V$$

Hence,

$$\frac{\rho C_p}{\beta}\frac{d}{dt}\delta V + V\left[\frac{\rho C_p \kappa}{\beta} - \frac{\delta V}{V}\right]\frac{dp}{dt} = -\oint_\Sigma \vec{q}\cdot\vec{n}\, dA + \int_R Q\, d\tau$$

For the system considered, assume $\frac{\delta V}{V} << 1$. Then

$$\frac{\rho C_p}{\beta}\frac{dV}{dt} + \frac{\rho C_p \kappa}{\beta} V \frac{dp}{dt} = -\oint \vec{q}\cdot\vec{n}\, dA + \int Q\, d\tau$$

We then have

$$\int_R Q(\vec{r},t)d\tau = P(t) = \oint \vec{q}\cdot\vec{n}\, dA + \frac{\rho C_p}{\beta}\frac{dV}{dt} + \frac{\rho C_p \kappa}{\beta} V \frac{dp}{dt}$$

If now we have a radioactive source of β and γ energy, the preceding considerations suggest a conceptual design of calorimeter as follows:

i) Provide a medium in R which is a good absorber of γ rays and whose thermophysical properties are well known. Mercury is a clear choice.

ii) Simultaneously measure the surface heat flow, the rate of volume dilation, and the rate of pressure rise, if any. The UCB calorimeter utilizes a constant pressure absorber.

The conduction calorimeter of Calvet-Tian type depends upon a measurement of surface heat flux be means of a thermopile surrounding the calorimeter vessel and uses twin vessels, one of which contains the sample to be observed and the other acting as a reference cell. The method is essentially quasi-steady as the power to the reference cell is controlled to maintain a balance of the two thermopiles. The measured power to the reference cell is the desired heat rate of the sample. Alternatively the thermopile emf may be used to measure the heat rate, in which case the reference cell is superfluous. The twin calorimeter usually exhibits faster response and is less sensitive to changes in the thermostat temperature.

The UCB calorimeter utilizes mercury as the gamma ray absorber. The dilatation of the mercury at constant pressure provides a prompt response measurement of energy desposited in the mercury and transferred to it as heat from the sample. The measured dilatation is the principal response at short cooling times. After considerable delay the heat is transferred via the thermopile to the thermostat. The classical Calvet-Tian twin cell was considered for this part of the measurement however due to the high cost of the thermopiles and reference heater control system it was elected to use the thermopile emf to indicate the heat flow.

Details of the calorimeter are described in the next section.

2. Description of the Calorimeter and Associated Equipment

2.1 General Features of the Calorimeter

The principle of operation of the calorimeter was described in the introduction. In this section the detailed design features will be presented. The components of the calorimeter are shown schematically in Fig. 1. The fissile sample is introduced into the tapered sample tube in the center of the cylindrical mercury absorber vessel. Water provides excellent thermal coupling between the sample and the sample tube to give rapid transfer of the beta energy, which is mainly deposited in the sample, to the sample tube and mercury absorber. The details of the sample tube are shown in Fig. 2.

The mercury vessel is held by a shrink fit of the aluminum thermostat block against the thermopile mounted on the cylindrical surface of the mercury vessel. The shrink fit provides radial compressive stress on the thermopile to assure good thermal conductance through the electrically insulated contacting surfaces. Details of the thermopile construction are given below. The mercury vessel measures 12.0 cm in diameter and 12.3 cm in length. The ends of the vessel are stiffened by fins to add rigidity to the envelope.

The cylindrical aluminum block measures 16.0 cm I.D., 26.9 cm O.D. and 25.5 cm in length. It is surrounded by a cylindrical lead shield 12.0 cm thick. These components were placed inside a thermostatically controlled and well insulated water bath. The thermostat controller used has a sensitivity of $\pm$ 0.001°C.

2.2 Dilatometer

The purpose of the dilatometer is to measure the change in stored energy within the mercury. For the particular characteristics of the decay heat from fission products the qualitative features of the mercury response are as follows. As soon as the fissile sample enters the calorimeter, energy from gamma rays is deposited directly in the mercury and the beta energy, which is completely

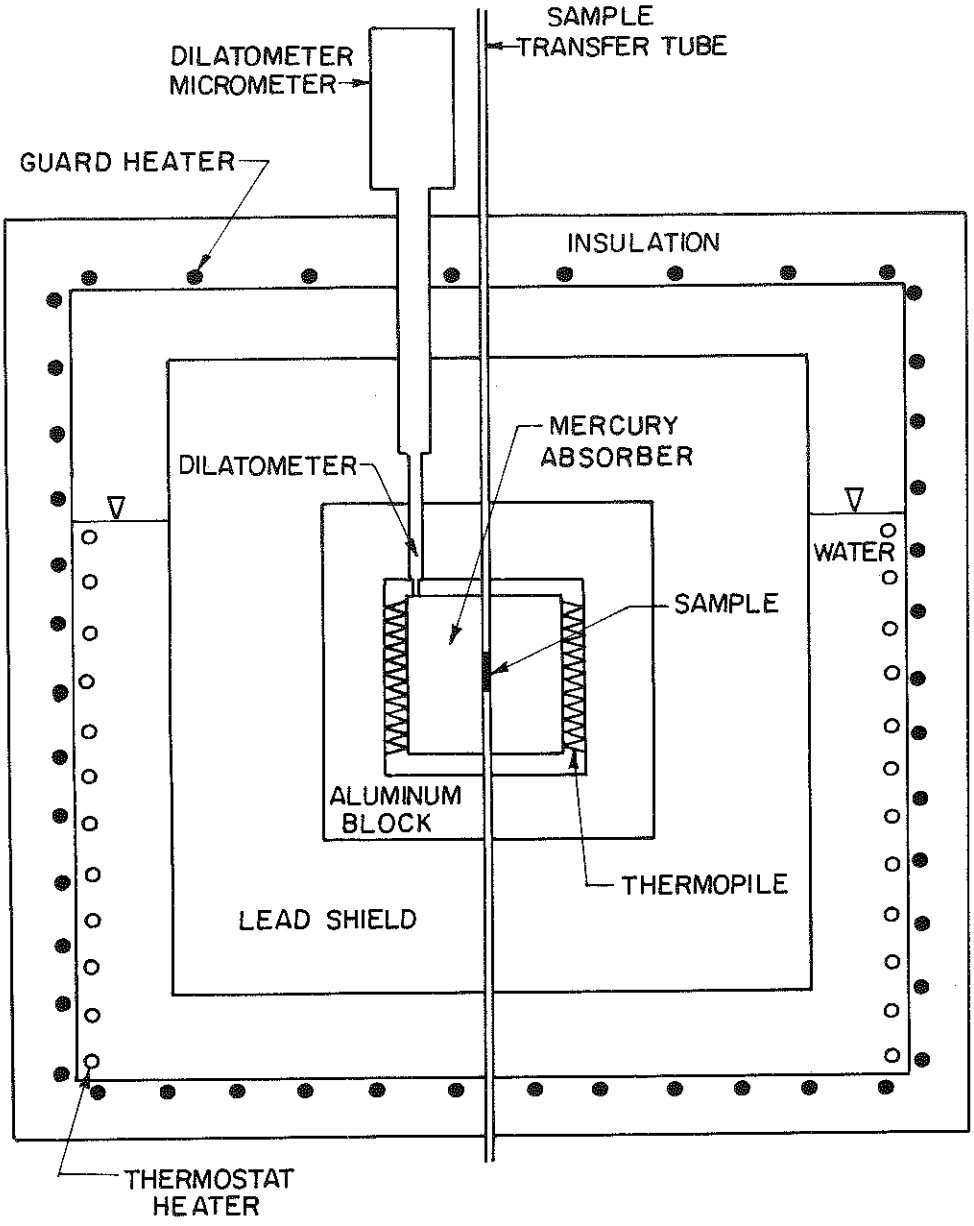

Figure 1 Schematic of the calorimeter

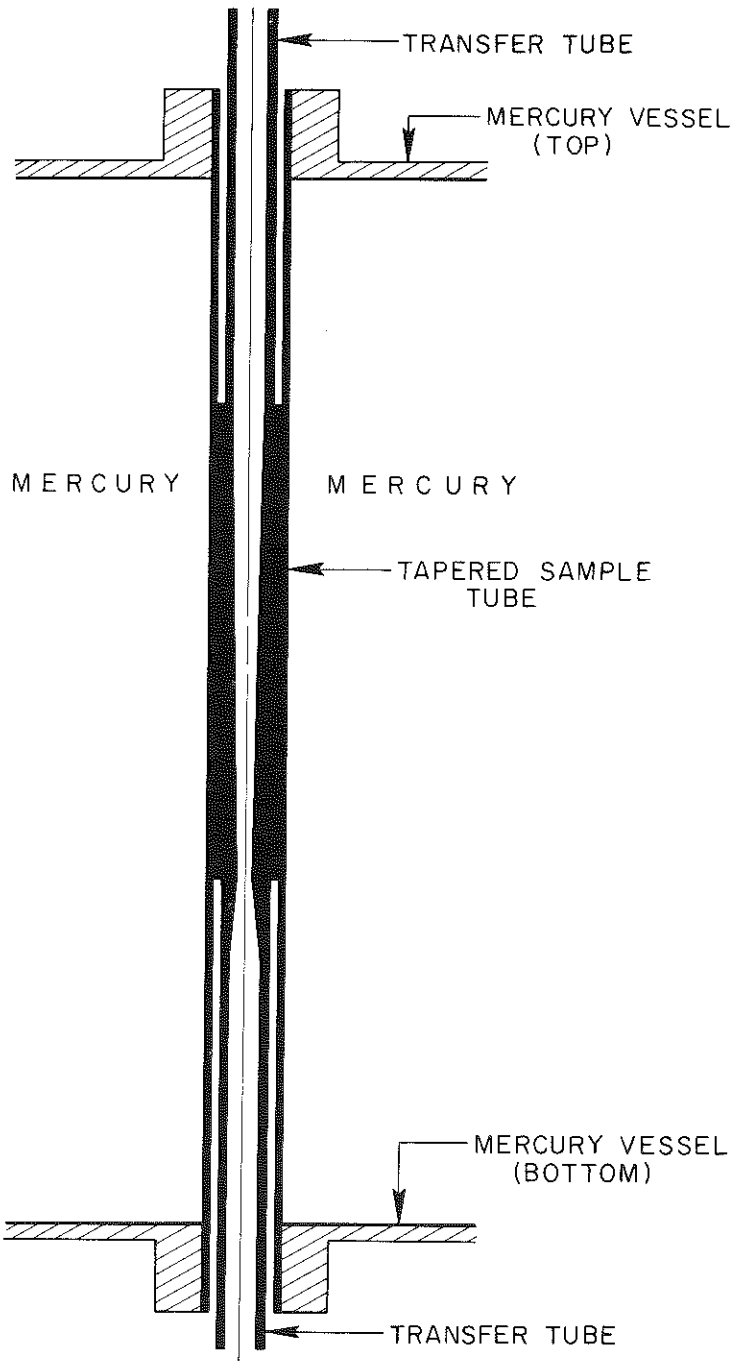

Figure 2 Sample tube details (not to scale)

deposited in sample (fuel and cladding) is transferred rapidly as heat to the mercury. At the start of the decay heat measurement the thermal expansion of the mercury is the measure of the total decay heat rate. When the outer surface of the mercury vessel rises above the initial calorimeter temperature, heat begins to flow through the thermopile. This heat rate, measured by the thermopile, represents an increasing fraction of the total decay heat rate as time goes on.

Eventually the decline in the decay heat rate causes the average mercury temperature to pass through a maximum and then fall slowly. Thus the rate of change of energy stored in the mercury plays some role, albeit an increasingly minor one as time goes on, throughout the entire measurement period. In order to design the dilatometer two aspects dominated the considerations. These were (a) the magnitude of the maximum volume increase expected and (b) the fraction of the maximum dilation that had to be detectable in order to achieve the desired goal for accuracy of the decay heat rate. Summation calculations were used to estimate the total decay heat rate and its gamma component. The gamma transport problem was solved using a Monte Carlo computer program to obtain a two dimensional (r,z) description of the time dependent distributed heat source in the mercury (and also to estimate the gamm leakage). This information was then used in a two spatial dimension transient heat conduction code to determine the transient temperature response. For a 24 hour irradiation of the samples selected it was predicted that the maximum volume increase of the mercury would be 1.67×10^{-2} cm^3 corresponding to a float displacement of about 4×10^{-2} cm.

Measurement of this small displacement was made using a fiber optics instrument, the model KD-100 Fotonic Sensor manufactured by MTI Instruments. This instrument can measure small surface displacements with a resolution of 1 micro-inch. The basis of its operation is the change in the amount of reflected light from the detected surface as the distance of separation changes. Its response

increases to a maximum and then falls as the distance of separation is increased. The response is nearly linear in the central portion of the increasing side of the curve. The configuration of the dilatometer adopted is shown in Figure 3. The sensor was mounted in an adjustable bellows that can be moved axially by a micrometer adjustment to position the optical head with a resolution of about 10^{-3} cm.

A stainless steel float was used in the mercury column. On the top of the float was mounted an optically flat front surfaced mirror. After filling the mercury vessel to the desired level the dilatometer cavity was evacuated and filled with argon gas to protect the mirror surface from possible oxidation. The float served as a platform for the mirror surface. To ensure that small changes in capillary wetting angle did not influence the level of floatation, dimensions were chosen for which the net capillary force has no influence. The force balance on the float is

$$\pi R_i^2 \rho g h + 2\pi R_i \sigma \cos\beta = \pi R_i^2 \rho_{H_g} g h_w + \pi R_i^2 \Delta p_c$$

where ρ is float density, ρ_{H_g} mercury density, σ is surface tension, β is contact angle, R_i and R_o are inner and outer radii of the annular meniscus (Figure 3) and

$$\Delta p_c = \frac{2\pi(R_i+R_o)\sigma\cos\beta}{\pi(R_o^2-R_i^2)} = \frac{2\sigma\cos\beta}{R_o-R_i}$$

Therefore

$$\frac{h_w}{h} = \frac{\rho}{\rho_{H_g}} - \frac{2\sigma\cos\beta}{h\rho_{H_g}} \left[\frac{1}{R_o-R_i} - \frac{1}{R_i}\right]$$

from which it is evident that the last term is zero when $\frac{R_i}{R_o} = \frac{1}{2}$. This simple analysis neglects the compound curvature of the meniscus but the effect on the results should be small.

In its final design the dilatometer has the ability to measure the maximum change in the stored energy with an accuracy between 1 part in 10,000 and 1 part

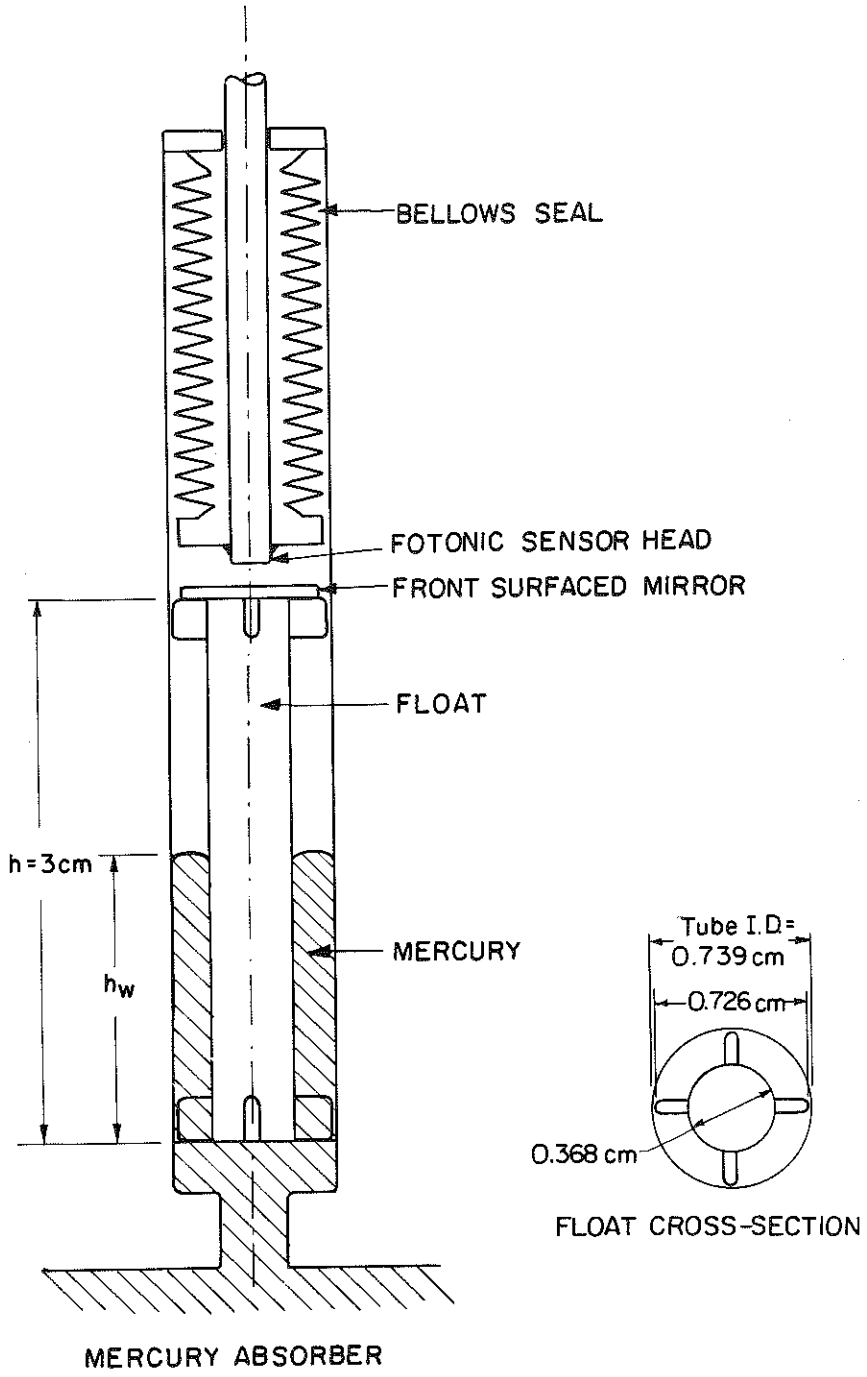

Figure 3 Schematic of the dilatometer

in 15,000 depending upon the duration of the irradiation. The Fotonic Sensor response was calibrated against the adjusting micrometer after installation in the dilatometer.

2.3 Thermopile

The thermopile design consists of a 1400 junction unit utilizing copper-constantan for its high Seebeck coefficient. Fabrication of a thermopile is one of the major challenges in calorimeter design. In the present application advantage was taken of the technology of electroplating of metals on plastics. Plastic (Nema G-10) bars 0.508 cm by 1.872 cm by 11.81 cm were used as the basic structural support. Small holes (28) were drilled diagonally through the width of the bars and 0.25 mm diameter constantan wires were epoxied into the holes with about 0.025 cm of bare wire extending on either side. The entire bar was then plated with copper about 0.8 mm thick. The irregular plating was then machined to a uniform thickness of 0.508 mm and slotted to produce 28 rectangular conducting elements connected by the diagonal constantan wires to produce a 28 junction thermopile. Fifty of these bars were cemented to the outside surface of the mercury vessel and connected electrically in series to form the 1400 junction thermopile. The space between the bars was then filled with epoxy and cured. After curing, the outside surface was finish machined for mating to the aluminum block. The aluminum block was anodized and shrink fitted onto the thermopile. Figure 4 is a photograph of the thermopile mounted on the mercury vessel. After assembly was complete it was found that one bar of the thermocouple was shorted to the mercury vessel. The thermopile was then rewired, bypassing the shorted element. A loss of sensitivity of the thermopile of 2% thereby resulted. Calibration of the thermopile will be discussed in a later section but it may be noted here that the pile sensitivity is in reasonable agreement with the known Seebeck coefficient of copper-constantan and the heat transfer analysis of the composite of the thermopile materials.

Figure 4 Photograph of thermopile on mercury vessel

2.4 Fissile Samples

The samples were fabricated by a specialist at Oak Ridge National Laboratory. The technique consisted of swaging aluminum tubes onto uranium wires. The end product was to be a completely sealed sample of the fissile material. All the samples were radiographed in two views taken at 90° to one another. Ten of the 23 samples were judged to have potential for fission product leakage. Of those samples used only one developed leakage of radioactivity.

Dimensions of the samples are given in Fig. 5. Due to the minimum practical uranium wire diameter, the desired ^{235}U content was obtained by using a 0.2 mm diameter uranium wire enriched to 40% in ^{235}U. The length of the 24 mg uranium wire is 4 cm while the total mass of the aluminum clad sample is nominally 1.02 g. The surface of each fissile sample was tapered to match the sample tube in the calorimeter and provide good thermal coupling. As shown in Fig. 5 the thicker end of the sample was designed with a nose cone shape to seat in an axially located support in the irradiation facility.

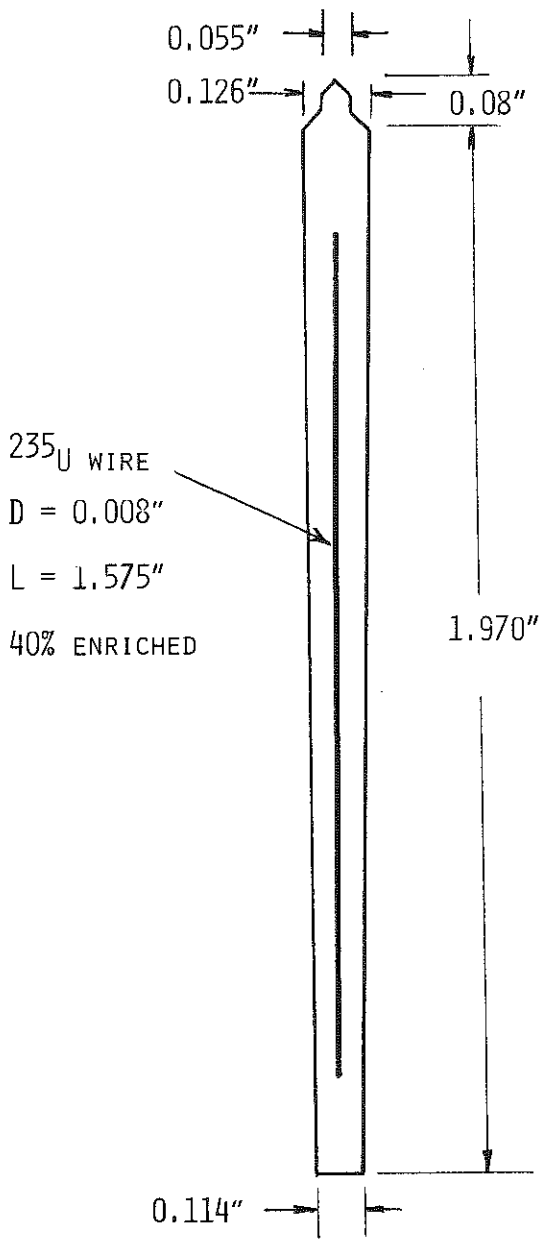

Figure 5 Fissile sample

2.5 Transfer System

A hydraulic transfer system was designed to provide rapid transfer of the sample from its irradiation position in the reacor into the calorimeter and to provide effective cooling of the sample during irradiation. The system consists of a closed loop of stainless steel tubing, a pressurizer, a circulating pump, several solenoid operated valves, a small heat exchanger and a spur line connected to the calorimeter. These components are shown schematically in Figure 6. All portions of the transfer system within the working area through which the irradiated sample passes enroute to the calorimeter were lead shielded.

During loading of the sample into the irradiation position and during the irradiation water is circulated through the loop by the pump at a nominal rate of 1.33 ℓ/min. The corresponding velocity in the transfer system tubing is 1.57 m/sec and in the annular passage cooling the sample is 3.29 m/sec. This flow produced a pressure drop of 2.3×10^5 N/m^2 (33.5 psi) in the 23 m long loop. The nominal fission power during irradiation, 38.5W, produces a surface heat flux on the sample of 10.2 W/cm^2. Steady state heat transfer analysis predicts a clad surface temperature of 47 C and a maximum fuel temperature of 52 C when the reactor pool water temperature is 42 C. Thus the cooling effectiveness is excellent during normal irradiation conditions. Additionally the thermal aspects of the safety analysis showed that the sample temperature would remain at a safe level even under accidental pump failure or loss of system pressurization (normally at an absolute pressure of 1.83×10^6 N/m^2 or 265 psia).

Transfer of the sample from the irradiation position to the calorimeter is accomplished automatically by an event sequence timer which provides the appropriate electrical signals to operate certain valves and switches. Starting the timer actuates the recording instrumentation and after a 120 second delay terminates power to the pump and actuates valves A and C (see Figure 6). This results in a pressure

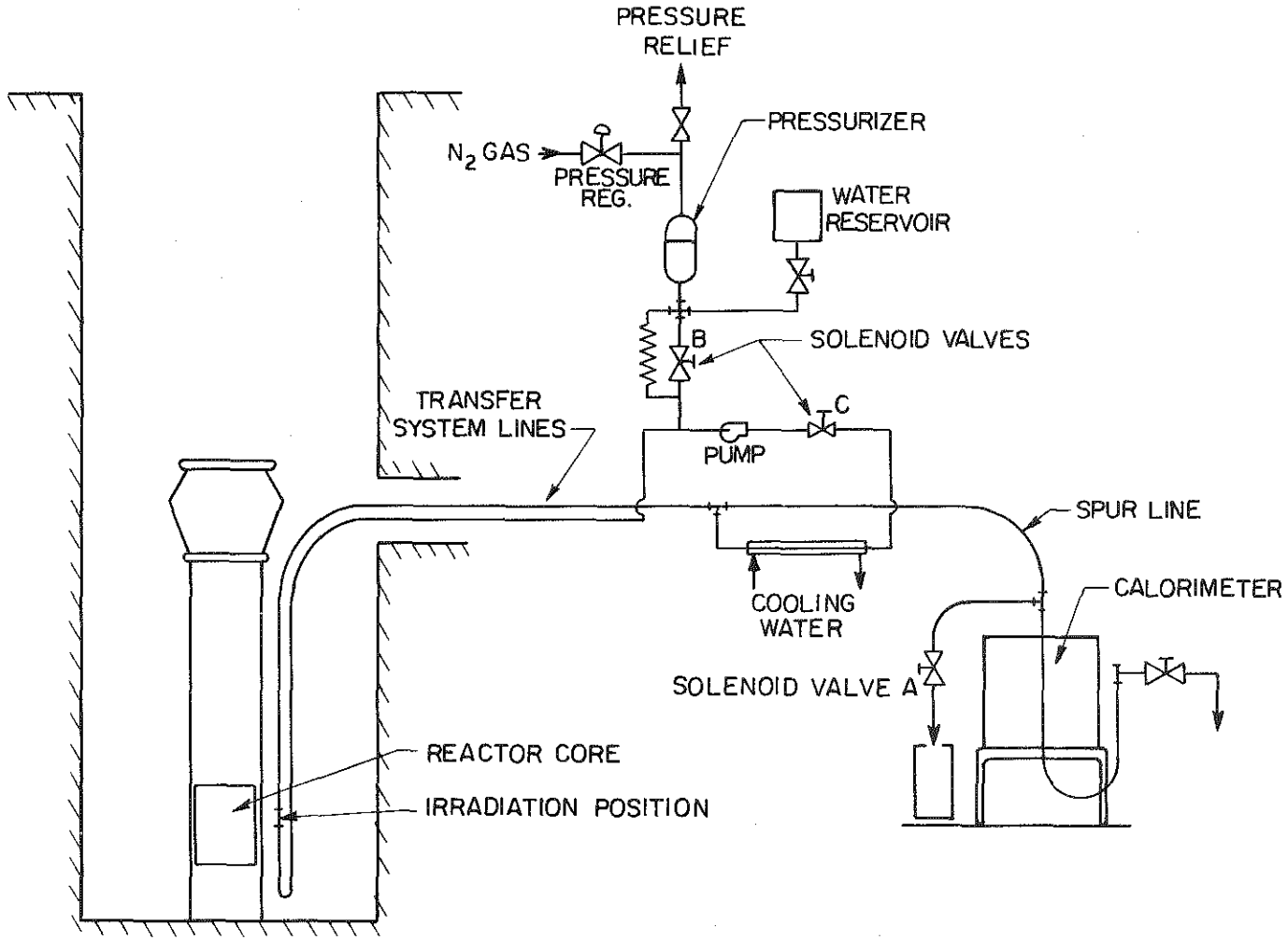

Figure 6 Transfer system

differential of 1.72 x 10^6 N/m^2 (250 psi) between the pressurizer and atmosphere acting to reverse the water flow and discharge to the atmosphere at the end of the spur line to the calorimeter. The purpose of valve B is to cause the water to pass through the parallel high resistance path and thereby decelerate the flow as the sample nears the calorimeter. When the sample reaches the "T" in the line above the calorimeter, it continues forward as a result of its inertia and gravity and falls into its seat in the calorimeter. Transient flow analysis predicted that the sample transport through the 13.5m distance to the calorimeter is accomplished in about 5 seconds. This prediction was verified experimentally.

2.6 Predicted Response of the Calorimeter

In order to select the instrument ranges for measurements, the dilatometer and thermopile responses to a decay heat measurement were predicted using the following assumptions:

- The decay heat and its characteristics (β and γ spectra) are given by the ORIGEN code. This gives a time dependent source condition.
- All β energy is deposited in the fuel.
- The spatial distribution of γ energy absorption is as predicted by the SAM-F Monte Carlo computer code (2 dimensional r,z).
- Heat transport within the calorimeter is by conduction.
- The thermopile conductance is known from its dimensions and materials properties.
- Initially the system is at uniform temperature.
- The boundary conditions include the constant thermostat temperature and the symmetry condition on the axis of the calorimeter.

A multiregion two dimensional (r,z coordinates) transient conduction computer code was used to calculate the transient temperature distribution within the calorimeter and from it the stored energy and the dilatation of the mercury were calculated. The surface temperature on the mercury vessel was used to

calculate the heat flow through the thermopile. Typical results of this calculation are shown in Figure 7 for a one day irradiation of a standard sample in a flux of 10^{14} n cm^{-2} sec^{-1}.

These predictions show that the dilatometer measurement accounts for essentially all the decay heat at very short cooling times (<10 sec). Power measured by the dilatometer falls off rapidly becoming zero at 250 seconds and then becomes negative and remains a negative contribution thereafter. This negative contribution represents the gradual cooling of the mercury as the decay heat source continues to decline.

The thermopile begins at zero and starts to rise at about 10 seconds. At 250 seconds, where the dilatometer measured contribution is zero, the thermopile measurement equals the total decay heat. At longer cooling times the thermopile measures a heat rate that is greater than the decay heat by the amount of the rate of loss of energy stored in the mercury.

2.7 Instrumentation

The dilatometer sensing element is the Fotonic Sensor described in an earlier section. The response of this instrument is zero when there is no gap, increases with increasing gap to a maximum and then diminishes with further increase in gap. It has been used on the small gap side of the peak response where the sensitivity is greatest. When the gap is set for peak response the output is adjusted to 10V. The gap is then adjusted to the desired position so that a suitable range of near linear response is available for the anticipated signal to be observed.

The thermopile output was fed to a Kiethly D.C. nanovoltmeter having volt range output. The outputs from the Kiethly, the Fotonic Sensor and two neutron monitors mounted adjacent to the sample in its irradiation facility and the outputs from several thermistor bridges used to monitor temperatures at key locations were all fed to an Autodata digital data aquisition unit and the digitized data recorded

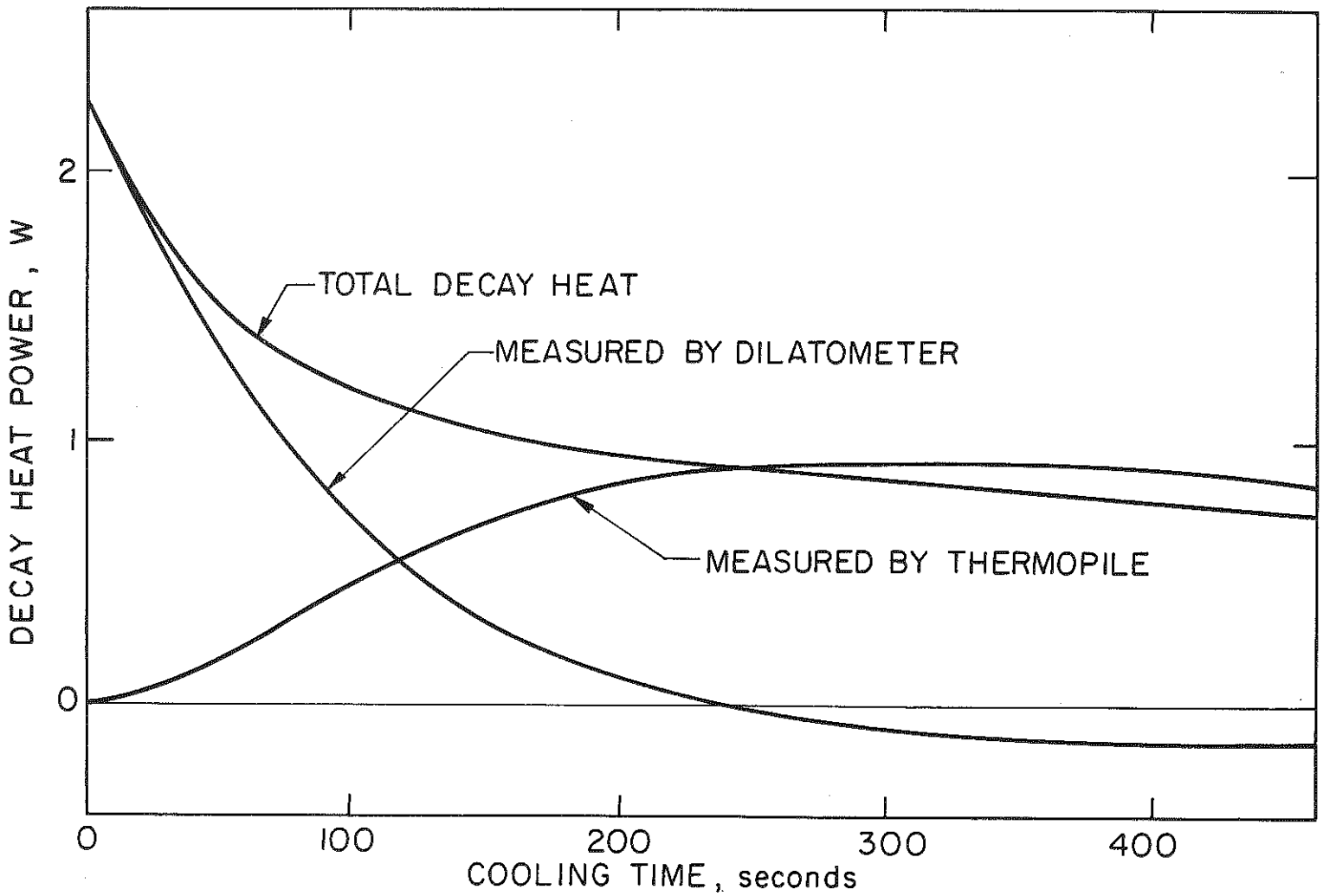

Figure 7 Theoretical response to decay heat

on magnetic tape. Using ten data channels the instrument is set for a 1 second scan rate during the first 600 seconds of a decay heat measurement and 1 minute scans thereafter.

2.8 Calibration Procedures

2.8.1 Fotonic Sensor

This instrument is sensitive to displacements that are smaller than readily available calibration standards. The sensing unit consists of a bundle of fibers that serve as light tubes. Light from a source in the instrument is transmitted through half the fibers and illuminates the observed surface. Reflected light is picked up by the other half of the fibers and provided the response signal. The normalized response curve is provided by the manufacturer. However for the present application it was necessary to do extensive additional calibrations using high precision micrometers (1/10,000 inch divisions) both on the bench in the laboratory and with the sensor mounted in the dilatometer. With considerable care extensive calibration data were obtained and smoothed to develop the calibration curve adopted for data reduction. Only data obtained in the dilatometer were used to develop the calibration curve since bench measurements tended to indicate the calibration may depend to a small degree upon the properties of the observed surface. The calibration is slightly nonlinear in the working range. It is stored in the data reduction code in tabular form (voltage vs. displacement) and log-log interpolation is used between points.

2.82. Calibration of the Calorimeter

The thermopile sensitivity may be measured in steady state tests using Joulean heating in place of the decay heat sample. These calibrations were conducted instead in the transient mode (step inputs in power) in order to simultaneously obtain direct calibration data for both the dilatometer and the thermopile.

The theoretically predicted response of the calorimeter to a step input (electrical) is shown qualitatively in Figure 8. The power is initially

measured by the dilatometer and then shifts to complete dependence on the thermopile as steady state is approached. The actual response was found to differ at early times in the transient as illustrated in Figure 9. The initial "bump" in the dilatometer response has been diagnosed as resulting from a small thermal strain in the central (sample tube) tube in the mercury vessel pressing against the ends of the vessel and increasing its volume very slightly. Thus mercury is drawn into the mercury vessel giving the appearance of a heat sink for a short period (approximately 4 to 5 seconds). A correction procedure was developed to account for this phenomenon in calibration tests and then applied to the decay heat data reduction.

Another difference in the actual response is the presence of a small amplitude wave superimposed on the thermopile signal. This is believed to be the result of a natural convection current within the mercury. According to the theory of the calorimeter this periodic component in the heat flow through the thermopile must be balanced by a similar component in the dilatometer response. However since it should appear as a small periodic component of the dilatometer response slope it is not easily seen visually in the experimental result.

Two precalibration runs and two post calibration runs were performed in the calorimeter with electrical step inputs ranging from 0.7 to 1.8 watts. The first step in the calibration data reduction involved rewriting the theoretical relationship from page 8 in the form

$$P(t) = - C_1 \frac{d\ell(t)}{dt} + C_2 V_{th}(t)$$

where $\ell(t)$ represents the position of the mercury level in the dilatometer and $V_{th}(t)$ represents the thermopile output voltage. The constants C_1 and C_2 represent the calibration coefficients for the dilatometer and the thermopile. The dilatometer response (voltage) was first converted to displacement $\ell(t)$ using the Fotonic Sensor calibration.

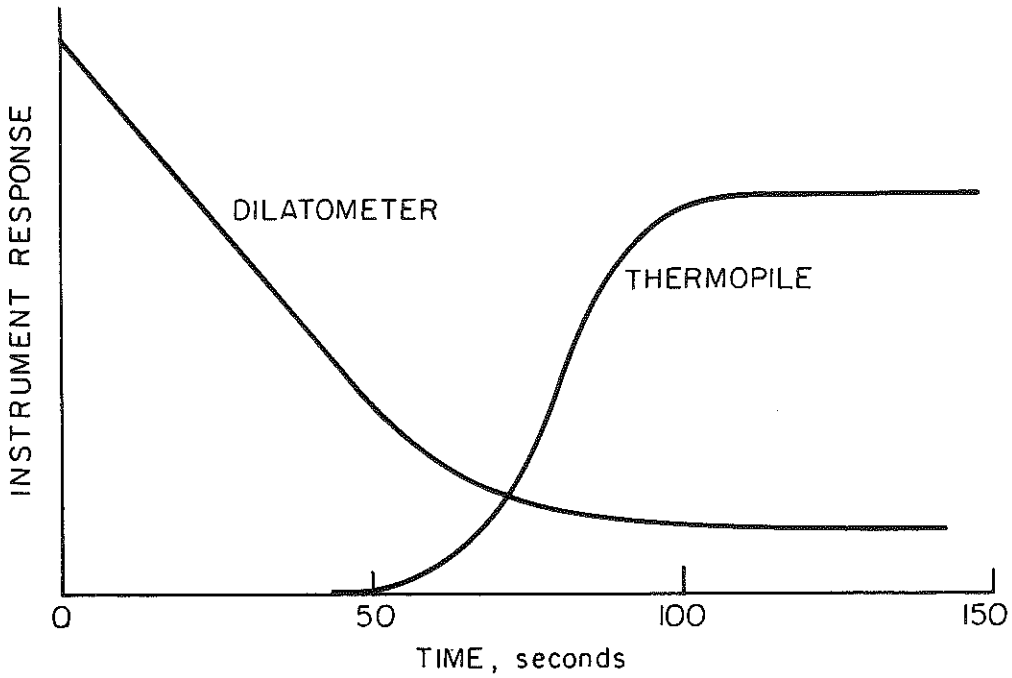

Figure 8 Theoretical response to step electric power input

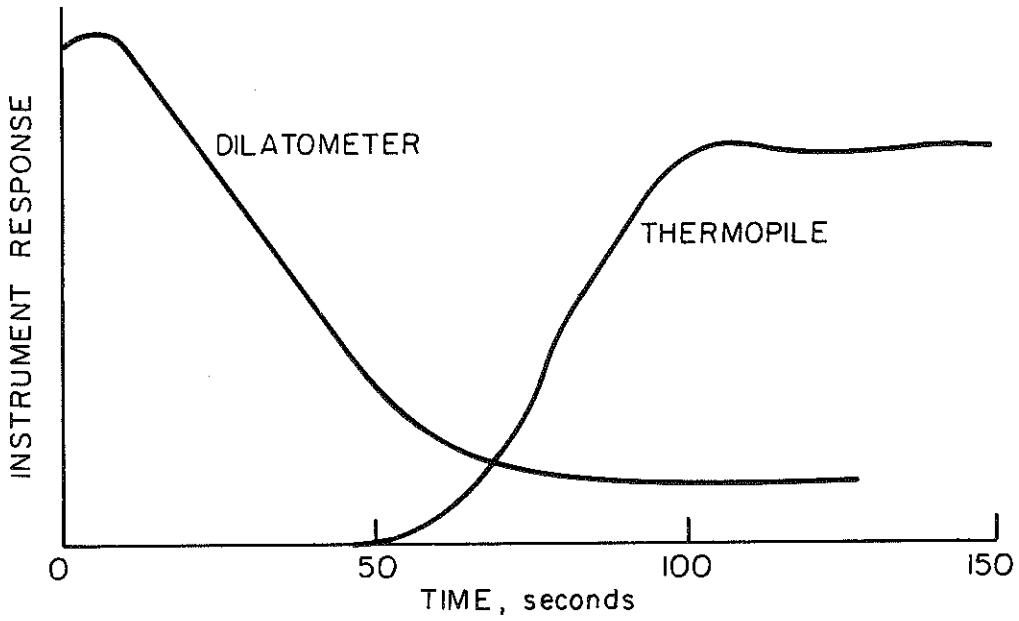

Figure 9 Actual response to step input

Next the theoretically predicted displacement $\ell_p(t)$ was compared with the calibration result and the difference

$$C(t) \triangleq \ell(t) - \ell_p(t)$$

was determined for each of the calibration runs. Since heat conduction and elastic deformation are linear phenomena it was proposed that the correction factor C(t) should scale to the power P. A general curve of $\frac{C(t)}{P}$ vs. time was developed from the four calibration runs. When this "normalized" correction factor was used in the data reduction procedure applied to calibration runs with theoretically determined values of C_1 and C_2 deviations of ±6% from the measured power were obtained. Small adjustments were then made iteratively in the constants to provide the best fit to the calibration data. The adopted values

$$C_1 = 4291 \quad \text{watts/cm}$$

$$C_2 = 1.368 \quad \text{watts/colt}$$

together with the adopted correction factor C(t) were then able to reproduce transient calibration data smoothly within ±2% over the entire transient.

When applying the normalized correction factor $\frac{C(t)}{P}$ to the decay heat data it was assumed that the power associated with heating of the central tube is the beta power only. Therefore P was taken, for each run, to be the time dependent beta power prediction from ENDF/B-IV summation calculations.

3. Irradiation Facility

The experiments were performed at the General Electric Companies Test Reactor (GETR) at the Vallecitos Laboratory, California. The transfer system and neutron flux monitors were mounted in a vertical pool facility tube near the reactor core. The facility tube was in turn mounted on "raft", a pantagraph like device that permits some radial movement of the facility tube and a resulting change in flux level of more than an order of magnitude. With the raft "full in" a well thermalized neutron flux of approximately 10^{14}n cm^2-sec is available.

GETR operates at steady power around the clock on a nominal 14 day cycle; 11 days at power plus 3 days for refueling. During the cycle flux shape is distorted by periodic movement of rod banks. The UCB experiment was irradiated at the vertical position least influenced by these distortions. In addition the rod banks were not moved during decay heat irradiations. Therefore the irradiations were accomplished at substantially constant flux; special care was exercised by the operators to hold the reactor power constant during the last hour of decay heat irradiations.

Heat rejection from the GETR is via a cooling tower and is somewhat influenced by changes in the weather. However the large thermal capacity of the system results in a gradual rise in pool water temperature over the eleven day operating cycle. The ambient temperature within the containment building where the calorimeter was located varied by about 10°C with weather changes. Both these features of GETR proved troublesome for sensitive calorimetry.

4. Experimental Procedures and Conditions

4.1 Procedures

Prior to the irradiation the calorimeter assembly is brought as close as possible to the temperature of the reactor pool (usually about 42°C and the system allowed to stablize). Stability is observed by recording on paper tape the signals from the Fotonic Sensor, the thermopile and transistors. The zero is adjusted on the Kiethly nanovoltmeter. The micrometer is adjusted to give the maximum output of the Fotonic Sensor. Its output is adjusted to 10.000 volts and the micrometer then adjusted to give an output of approximately 8 volts. This setting is chosen as the beginning of the nearly linear range of the Fotonic Sensor output and should give maximum accuracy and sensitivity in the results.

When the calorimeter has stablized, the position of the raft is confirmed with reactor operators, and permission is obtained to load the sample into the transfer system. This is done by opening the fittings on the "T" connecting the loop to the calorimeter spur and inserting the sample with its "nose" toward the reactor. The pressurizer is filled with water and after the sample is inserted a low gas pressure is applied to the pressurizer and a small amount of water bled from the system to remove any air that may have been trapped in the loop during sample loading.

After checking the loop for tightness the system pressure is set at the operating level 1.83×10^6 N/m^2. The transfer system controller panel is then energized and after obtaining permission from the reactor operator the sample is moved to the irradiation position by turning on the pump for several short periods ($\sim$1 second) to allow the sample to seat gently into its support. The pump is then left running and the time of starting irradiation is recorded.

One hour prior to the end of irradiation all instrument settings are checked once more. The Autodata is set on 10 minute scan and recording is on paper tape. The magnetic tape is loaded into the recorder. Twenty minutes prior to transfer the Autodata is placed on continuous scan. Ten minutes prior to transfer all personnel

are cleared from the vicinity of the transfer lines and calorimeter and the radiation monitor checks his survey instruments.

Two minutes prior to the desired transfer time, the controller is switched to "Transfer Enable". This allows the experimenter two minutes to leave the area before the sample is automatically transferred and data recording initiated. Arrival of the sample in the calorimeter is confirmed by thermal response and area radiation monitors. After a few minutes it is safe to approach the calorimeter and the water ejected from the transfer system is checked for radioactivity.

The data collection process continues automatically for 24 hours. At the end of this time the transfer line spur is disconnected from the cooling loop and connected to a shielded transfer line leading to a shipping cask. The sample is moved to the shipping cask by means of a long wire that is inserted through the bottom of the calorimeter to push the sample. The calorimeter is then prepared for the next test. Samples are subsequently shipped to Berkeley where the number of fissions is measured as described below.

4.2 Experimental Conditions

A total of 12 experiments were conducted, four each at irradiation times of 1, 4 and 24 hours. The runs are numbered in chronological order. Their nominal irradiation times are as follows:

Irradiation Time, hrs	Run Numbers
1	1, 2, 11, 12
4	3, 4, 9, 10
24	5, 6, 7, 8

Three of the runs were irretreivably lost. During Run 5, the sample was accidentally transferred as maintenance was being performed on the instrumentation. In Run 7 the delay timer malfunctioned ejecting the sample immediately upon setting "Transfer

Enable" and the same electrical difficulty caused the scan signal to fail. Run 11 was aborted when the sample was found to be leaking fission products.

All the remaining runs were reduced, although some gaps occurred in some data at some cooling times due to instrument difficulties. Finally Runs 2 and 10 were discarded because they produced improbable oscillatory results.

The measurement of total fissions in each sample is described in the next section.

5. Fission Rate Measurements

5.1 Fission Rate Monitoring During Irradiations

To facilitate data analysis and interpretation, it is desirable to maintain a constant fission rate over the duration of the irradiations. This is especially important over the last part of the irradiation where changes in fission rates can cause appreciable variation in the contribution to total decay power from the shorter-lived fission products. Comparison of the calculated decay powers from samples subject to step function and periodic changes in fission rates with those from constant fission rates showed that for variations typical at GETR, negligible difference existed so long as the fission rate during the last 20 minutes was maintained at the average level of the preceding part of the irradiation. To insure this characteristic, signals from monitors were used to determine the average fission rate and to adjust the reactor power level when necessary.

The irradiation conditions were monitored with a miniature fission chamber (Reuter Stokes Model RS-C6-0201-221) and a rhodium self-powered detector (Reuter Stokes Model RS-N-202-M1), both of which were located adjacent to the sample irradiation position with axes parallel to the sample asix and positioned symmetrically with respect to the median plane of the sample. The fission chamber was the primary monitor and the self-powered detector was used only as a backup device in the event of failure or drift in the fission chamber output. Signals from the two detectors were amplified and processed with the AUTODATA analyzer. Initial tests with the detectors showed that both operated stably and gave flux values within calibration uncertainties specified by the manufacturer (±20%).

For each run the outputs from the detectors were sampled at one minute intervals beginning 5-10 minutes prior to sample insertion and continuing throughout the irradiation. (For runs of long duration, the sampling interval was increased to 5 minutes during the mid-part of the irradiation.) Approximately 20 minutes prior to the expected end of irradiation, the averages of the detector signals were calculated and adjustment in reactor power level requested if necessary to insure equality with the average during the remainder of the irradiation. The time variations of the signal from the fission chamber from all runs are shown in Figures 10 and 11. Typically, the variations during one and four hour irradiations were less than 2% from the mean and for Run #06 which was irradiated for 22.25 hours, the average value for the last twenty minutes was identical to the average from the preceeding part within statistical errors (1.3%).

5.2 Counting System

Gamma rays from the fuel samples were counted with the system shown schematically in Figure 12. The Ge(Li) detector (ORTEC Model VIP) exhibited a resolution of 2 keV (FWHM) and a peak-to-compton ratio of 33 at 1.332 MeV. Line shapes were within 10% of gaussian to about 1/50 of the peak amplitude. The detector was partially shielded by 2 inches of lead to reduce background. Because of the strength of the fission

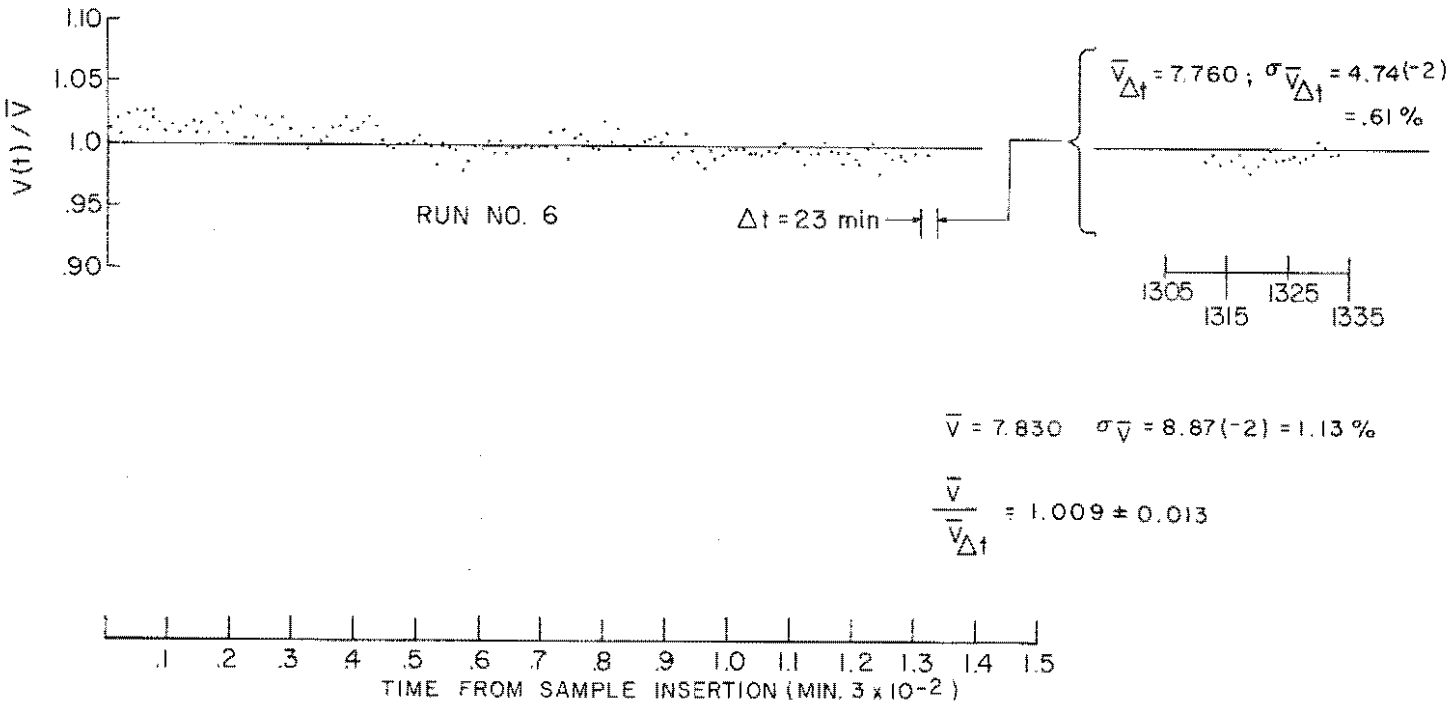

Figure 10 Variation in neutron flux, 22.3 hour irradiation

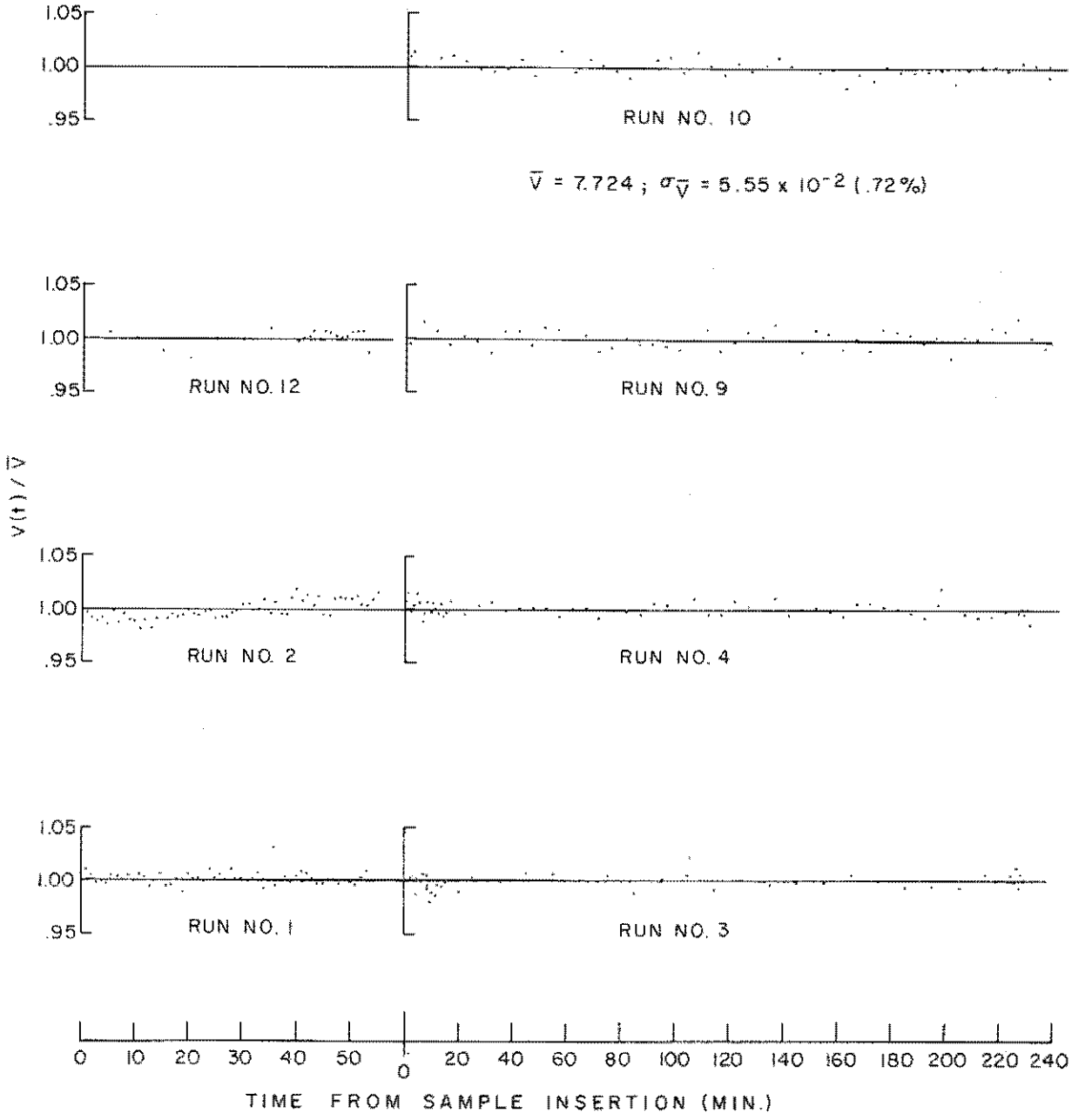

Figure 11 Variation in neutron flux, 1 hour and 4 hour irradiation

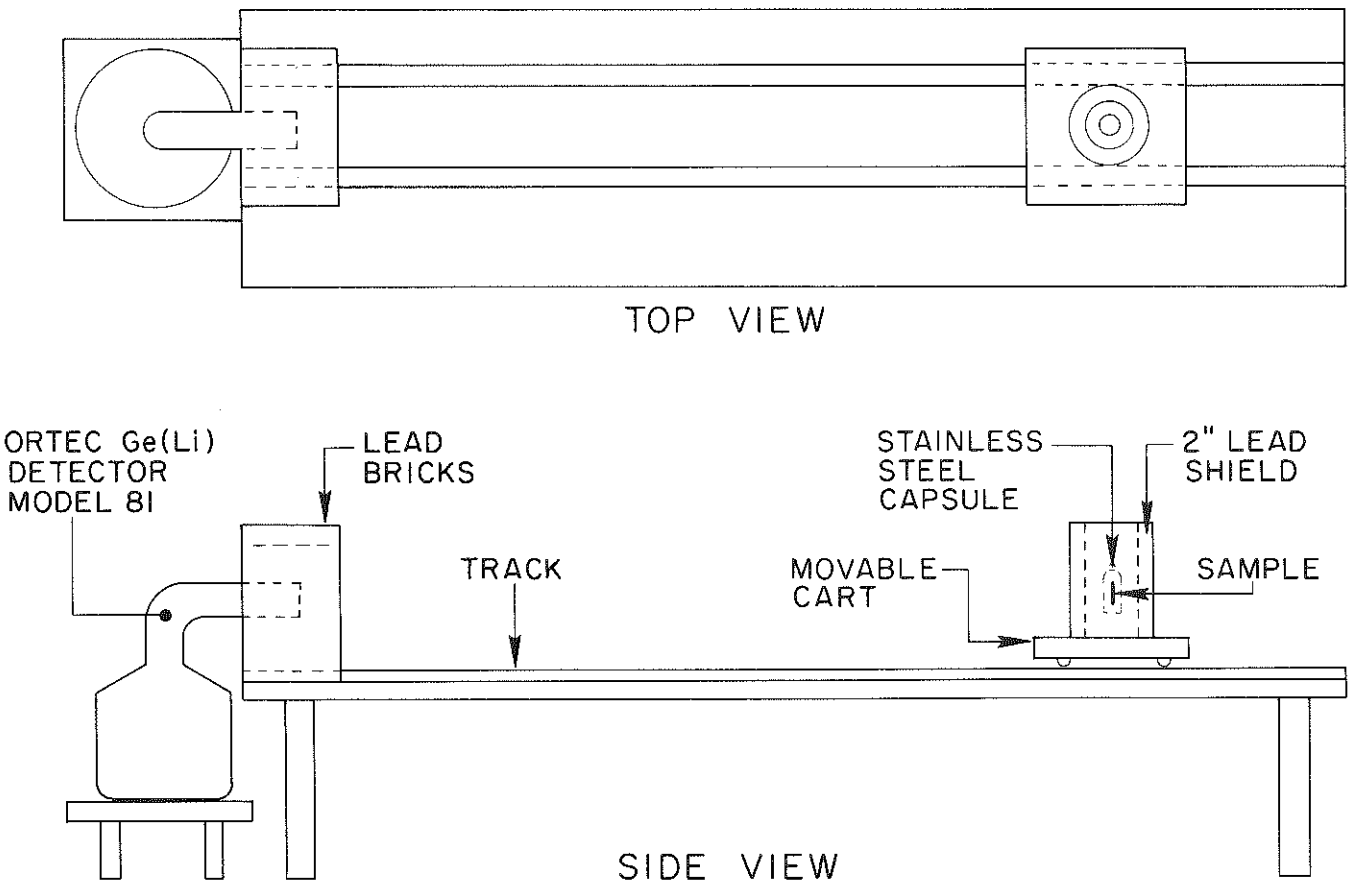

Figure 12 Fission assay counting system

product sources all samples were counted within their stainless steel transport capsules which were positioned on axis to the detector within a 2" cylindrical lead shield fixed on the moveable cart shown in Figure 12. The radial separations of sample and detector were adjusted to give about the same input rates into the detector ($(1\text{-}2)\times10^{3}$ sec^{-1}) in order to minimize errors due to pulse summing effects. To obtain absolute γ-decay rates from the samples, measured intensities were corrected for shielding, radial separation between source and detector, and the absolute detector efficiency. The factors involved in this process are discussed below in detail.

1) Absolute Detector Efficiency:

The absolute efficiency of the Ge(Li) detector as a function of γ-ray energy was obtained primarily through standards obtained from the LABORATOIRE DE MÉTROLOGIE DES RAYONNEMENTS IONISANTS, COMMISSARIATE À L'ENERGIE ATOMIQUE, France. The sources were approximate point sources (ϕ<2 mm) sealed between thin plastic films ($\sim$24 mg cm^{-2}) which were mounted in plastic rings. The sources were calibrated in γ min^{-1} with uncertainties of <1.5% at the 99.7% confidence level. The sources were mounted at 21.80 ± 0.05 cm from the face of the detector encapsulation for measurement of the absolute detector efficiency. In addition to these sources, extension of the efficiency curve to higher energies was obtained with an absolute calibrated source of ^{60}Co (Isotopes Products Laboratories) and a course of ^{24}Na (for relative

intensities of E_γ = 1368 and 2754 keV). All absolute sources were corrected for decay and analyzer deadtime and the efficiency curve from these was used to normalize the relative efficiencies from ^{24}Na decay.

As expected the variation of efficiency with energy in the range E_γ > 600 keV was quite simple. In Table 1 are given the absolute efficiencies obtained with these sources and a comparison with the values obtained by a linear fit to the logarithms of the data point coordinates. Clearly, the data are well reproduced by the fitted curve and lend confidence to the quality of the data with respect to the relative efficiencies. The mean absolute deviation of the data points from the fitted curve is within about $0.2\overline{\sigma}$. Based on these data, the fitted curve was used to calculate the efficiency at 1368 keV and the relative efficiences from the ^{24}Na measurement were used to extend the efficiency curve. The overall results were then used to provide absolute efficiencies for the γ-rays from ^{95}Zr and ^{140}(Ba-La) as given in Table 2.

2) Shelf Factors:

Correction of γ-ray emission rates for the solid angle variation between the sample position and the position at which the detector was absolutely calibrated was obtained by relative interaction rates with point sources of ^{60}Co in the range 22 - 60 cm,

Table 1

Absolute Detector Efficiencies and Comparison with Fitted Curve

E_γ (keV)		$\epsilon ff(\Delta\epsilon ff)x10^4$ [a]	$\epsilon ffx10^4$ [b]	$\Delta(\%)$ [c]
59.55	^{241}Am	13.68 ± 0.33		
88.01	^{109}Cd	15.25 ± 0.25		
121.97	^{57}Co	16.18 ± 0.27		
136.33	^{57}Co	14.68 ± 0.26		
165.85	^{139}Ce	13.48 ± 0.20		
279.19	^{203}Hg	8.213 ± 0.206		
391.69	^{135}Sn	6.086 ± 0.206		
514.00	^{85}Sr	4.287 ± 0.117	4.334	+1.10
661.63	^{137}Cs	3.475 ± 0.053	3.440	-1.01
834.83	^{54}Mn	2.745 ± 0.042	2.760	+0.55
1115.52	^{65}Zn	2.110 ± 0.032	2.098	-0.57
1173.23	^{60}Co	1.993 ± 0.028	2.000	+0.34
1332.50	^{60}Co	1.769 ± 0.025	1.773	+0.21

a/ from absolute standards

b/ from linear fit to log ϵff vs log E_γ; average of two curves calculated with and without the data point for E_γ = 514.00 keV (^{85}Sr).

c/ $\Delta = \left(\frac{\epsilon ff^{(2)}}{\epsilon ff^{(1)}} - 1\right) \times 10^2$

Table 2

Absolute Detector Efficiencies for Gamma Rays from ^{95}Zr and ^{140}(Ba-La)

E_γ(keV)	Source	$\varepsilon ff(\Delta\varepsilon ff)x10^4$ [a/]
724.18	^{95}Zr	3.158 ± 0.022
756.71	^{95}Zr	3.030 ± 0.021
815.83	^{140}(Ba-La)	2.821 ± 0.019
925.23	^{140}(Ba-La)	2.504 ± 0.018
1596.20	^{140}(Ba-La)	1.494 ± 0.010

a/ The errors shown are based on the average absolute deviation of the points given in Table 1.

and by use of shielded fission product sources in the range 40 - 214 cm. Sources of different strengths were chosen to maintain sufficiently low input rates ($<2\times10^3$ sec^{-1}) to minimize pulse summing effects. The data were then fitted with an equation of the form

$$\log(SF) = a + b \log r + c (\log r)^2$$

in order to account for the departures from the $1/r^2$ law at small distances. This form provided an excellent representation of the data over the entire range and gave a mean absolute deviation of the curve from the fitted points of 0.7%. The data were then normalized to the absolute efficiency at the calibration position.

3) Shielding Factors:

In order to obtain overall shielding factors for the lead shield and the stainless steel capsules, several samples were counted both in the shields and as bare wires. In all cases the lead shield was fixed in the same position on the moveable support and only the radial distance between the source and the detector was varied. We have assumed that the stainless steel capsules were identical. The shielding factors for the γ-rays from decay of ^{95}Zr and ^{140}(Ba-La) were obtained from pairs of measurements on samples 1, 2 and 12. The data are shown in Table 3. In order to observe possible systematic errors, the errors shown for the shielding factors are statistical fitting errors only as obtained from the computer fit. The results from samples R01 and R02 are in excellent agreement with one another and in moderate agreement with those obtained from sample R12.

Table 3

Shielding Factors for Gamma Rays from ^{95}Zr and ^{140}(Ba-La)

E_γ	Shielding Factors and Errors (%)[a/] R01	R02	R12	$\overline{SF}$(01,02)
725	520.0 (0.6)	515.6 (0.2)	545.3 (1.1)	517.8 (0.43)
757	401.0 (0.6)	398.1 (0.6)	397.9 (2.0)	399.5 (0.36)
816	257.9 (1.3)	260.5 (1.4)	236.2 (6.2)	259.2 (0.50)
925	139.0 (2.8)	154.6 (2.0)	147.2 (2.2)	146.8 (5.6)
1596	32.09(1.0)	31.84(1.2)	32.84(0.6)	31.96(0.39)

a/ Errors represent average statistical errors only.

The latter have considerably larger statistical errors on the average even though the total areas of peaks are comparable to those from the other runs. Experinece has shown that this is generally observed when the line shapes are poorer or the spectrum is more complex in the vicinity of the lines. Because of the better quality of the fits from samples R01 and R02, we believe that the average shielding factors from these measurements are more reliable. It is clear, however, that the agreement between all sets of measurements for the γ-rays at 757 and 1597 keV is excellent and these γ-rays should provide the most reliable estimates of fission rates in these measurements.

4) Constancy of Shielding Factors:

All samples were counted in the 2" cylindrical lead shield which was fixed relative to the moveable cart. Thus the constancy of the shield factor for all samples depends on the constancy of the shielding of the stainless steel capsules in which the fuel samples were located. To insure this, all capsule bodies were machined from the same stock and dimensions were kept within approximately 10^{-3} inches. Each body and cap was weighed individually and these were matched to minimize the variation in total capsule mass. The data are given in Table 4. The maximum deviations in the masses of the bodies, caps and total capsule were 1.8×10^{-1}%, 5.1×10^{-1}%, and 4.2×10^{-2}%, respectively. Since the principal part of the shielding is due to the body, the deviation in body mass is sufficiently small to insure that, apart from possible material nonuniformity, the assumption of constancy in capsule shielding is quite good.

Table 4

Deviation of Masses of Stainless Steel Capsules

Run No.	ΔBody Mass^{+}(%) [a/]	ΔCap Mass^{+}(%) [b/]	ΔTotal Mass^{+}(%) [c/]
01	0.00	0.26	0.00
02	-0.088	0.30	0.0004
03	0.063	0.002	-0.0012
04	-0.021	0.35	0.0017
06	0.11	-0.13	0.0098
08	0.0048	0.18	-0.013
09	-0.0078	0.29	-0.013
10	0.094	-0.045	0.014
12	-0.069	0.38	-0.032
Maximum Δ =	0.18	0.51	0.04

a/ Relative to body mass of 604.29 gm

b/ Relative to cap mass of 149.36 gm

c/ Relative to total mass of capsule for Run 01.

5.3 Summary of Sample Fission Rates:

Fission rates for all samples were calculated as average values from assay of the disintegration rates of ^{95}Zr and ^{140}(Ba-La). Based on examination of the spectral distributions in the vicinity of full energy peaks and the quality of computer fits, the most accurate assays were derived from the γ-rays at 724 and 757 keV (^{95}Zr) and 1596 keV (^{140}(Ba-La)). The decay and fission yield parameters used for the calculations are given in Table 5. The majority of the decay data were taken from the evaluation of Helmer and Greenwood and we have found that the relative intensities of the two lines from ^{95}Zr decay gave quite consistent results for the absolute disintegration rate within statistical fitting errors in all cases where the lines appeared well resolved and strong compared to the underlying compton distributions. Typically, however, the line at 757 keV provided slightly more precise results. The fission yeilds were taken directly from the 1974 compilation of Meek and Rider, and the errors shown in the table are the mean values of the error ranges given by these authors.

Mean fission rates were calculated from the appropriate Bateman equations for growth and decay during and after irradiation. The associated errors ($\pm 1\sigma$) were calculated by an exact variance algorithm assuming the errors in each parameter to be independent. These results are compiled in Table 6. All samples were assayed twice at times separated by 1 - 2 months and examination of the data shows excellent agreement between the individual

measurements. For essentially all individual measurements the agreement is within ±1σ which is less than 3%. Included in the table are average values of fission rates based on assay of ^{95}Zr or ^{140}(Ba-La). Due predominantly to the small error in the absolute γ-ray abundance, fission rates obtained from the decay of ^{140}(Ga-La) have somewhat smaller errors (∿2.36%). No significant systematic difference between the latter and the values derived from ^{95}Zr were evident.

In order to assess possible systematic errors in our measurements, the fuel sample from Run No. 02 was sent for independent assay to the Radiochemistry Division at the Lawrence Livermore Laboratory (LLL) and the Los Alamos Scientific Laboratory (LASL). At LLL, the sample was counted with a standard Ge(Li) spectrometer system normally used in fission rate measurements and the intensities of transitions from ^{95}Zr and ^{140}(Ba-La) were assayed. No corrections were made for attenuation in the wire and these measurements then served as a check on our absolute γ-ray measurements. Following the LLL measurements, the sample was shipped to LASL where it was subjected to a radiochemical separation procedure for direct assay of ^{140}Ba by β-ray measurement. Measurement of ^{95}Zr γ-ray intensities were also obtained on an aliquot of the dissolved sample. Comparison with this result provides an assessment of possible bias due to correction for attenuation of photons in the fuel samples and due to the fission yields and γ-ray abundances used in our work. These comparisons are summarized in Table 7. The absolute γ-disintegration rates as measured at LLL and UCB agree within the quoted errors (±1σ) for the γ-rays at 724 and 1596 keV, but differs by about 2σ for the γ-ray at 757 keV. Examination of the relative γ-ray intensities indicates that again agreement between data for the 724 and

1596 keV transitions is within ±1σ indicating no appreciable bias in the shape of the relative efficiency curves of the γ-ray spectrometers. Based on the evaluated data of Helmer and Greenwood the ratio of the absolute intensities of the two γ-rays from ^{95}Zr decay is $I_\gamma(757)/I_\gamma(724) = 124.0 \pm 1.80$ which clearly overlaps with both sets of measurements and we therefore conclude that no bias in the shapes of the effeciency curves exists and that the differences in mean values of the γ-ray intensities must be due to statistical fitting and uncertainties and absolute efficiency calibrations. The unweighted average of the intensity ratios $I_\gamma(LLL)/I_\gamma(UCB)$ is 1.24 ± 0.023 and indicates excellent agreement within the estimated uncertainties.

The absolute average fission rates as determined by the LASL and UCB measurements on ^{140}(Ba-La) decay for this sample are in excellent agreement, the mean values differing by less than 1%. In assessing possible systematic uncertainties in the LASL measurements, we note that comparison of γ-ray intensities from a fission source measured at LASL and at Idaho by R. L. Heath yielded differences in mean values of about 0.7%. Taken together, the agreement between the independent assays indicates that no systematic errors are peculiar to our measurement technique.

In table 8 are listed the adopted values of fission rates and errors for each fuel sample. The adopted values are the means of the rates given in the last two columns of Table 6. In arriving at error estimates we have quoted the larger of the standard deviations calculated from the set of all measurements for a given sample (method A) and calculated from the data in the last two columns of Table 6 under the assumption that measurements based on assay of ^{95}Zr and ^{140}(Ba-La) can be treated as independent (method B). The errors obtained from method A ranged from much smaller than to about the same magnitude as those from method b except for runs No. 6. In this case the data seem to possess less internal consistency.

Table 5

Decay Properties[a] of ^{95}Zr and ^{140}(Ba-La) Used in this Study

	Isotopes		
	^{95}Zr	^{140}Ba	^{140}La
Half-life	(64.4 ± 0.5)da	(12.70 ± 0.01)da	(40.26 ± 0.02)hr
γ-ray energy (kev)	724.18		815.83
Absolute Intensity (%)	(44.3 ± 0.5)		(22.58 ± 0.60)[b]
	756.71		925.23
	(54.8 ± 0.5)		(7.1 ± 0.3)[b]
			1596.20
			(95.33 ± 0.16)
Fission Yield (%)	6.549 ± 0.115[c]	6.316 ± 0.107[c]	(5.7 ± 0.6)x10^{-1}[c]

a/ Unless otherwise noted, all data were obtained from the evaluated decay scheme data of R. G. Helmer and R. C. Greenwood, Nucl. Tech. 25, 258 (1975)

b/ Average values from the recent data files of the Table of Isotopes Project, Lawrence Berkeley Laboratory, December, 1976 (not evaluated).

c/ Obtained from "Compilation of Fission Product Yields, Vallecitos Nuclear Center, 1974", by M. E. Meek and B. F. Rider, General Electric Report NEDO-12154-1, 74 NED6, January, 1974 (see text).

Table 6

Summary of Fission Rates Assayed Through Decay of ^{95}Zr and $^{140}(Ba\text{-}La)$

Run No.	Code	t_{irr}(hr)	$[R_f(E_\gamma)(\Delta\%)sec^{-1}] \div 10^{12}$ [a/] E_γ = 724 keV	E_γ = 757 keV	E_γ = 1596 keV	$[R_f(^{95}Zr)sec^{-1}] \div 10^{12}$ [b/]	$[\bar{R}_f(^{140}Ba)sec^{-1}] \div 10^{12}$ [b/]
1	01-2	1.00	1.129 (2.92)	1.131 (3.84)	1.133 (2.21)	1.128 (2.78)	1.131 (2.08)
	01-1		1.124 (3.00)	1.126 (2.91)	1.129 (2.28)		
2	02-5	1.00	1.134 (2.92)	1.126 (2.84)	1.139 (2.17)	1.132 (2.77)	1.141 (2.15)
	02-3		1.139 (2.94)	1.130 (2.91)	1.143 (2.43)		
12	12-4	1.00	0.9189(3.00)	0.9402(2.98)	0.9328(2.18)	0.9438(2.96)	9.9522(2.39)
	12-3		0.9730(2.96)	0.9449(3.37)	0.9695(2.14)		
	12-1		0.9288(3.20)	0.9570(2.98)	0.9543(2.83)		
3	03-2	4.00	1.088 (2.95)	1.100 (2.81)	1.089 (2.20)	1.129 (2.87)	1.104 (2.09)
	03-1		1.123 (3.03)	1.204 (3.20)	1.119 (2.30)		
4	04-4	4.00	1.094 (2.95)	1.093 (2.89)	1.111 (2.20)	1.098 (2.81)	1.115 (2.09)
	04-3		1.109 (2.99)	1.094 (2.93)	1.120 (2.32)		
6	06-3	22.25	0.8868(2.98)	0.8955(2.88)	0.8684(2.18)	0.9114(2.94)	0.8888(2.20)
	06-1		0.9333(3.04)	0.9302(2.89)	0.9092(2.22)		
8	08-2	22.35	1.006 (2.96)	1.007 (2.88)	1.015 (2.17)	1.006 (2.95)	1.024 (2.19)
	08-1		1.009 (3.04)	1.003 (2.91)	1.033 (2.21)		
9	09-2	4.00	0.9947(3.01)	0.9866(2.89)	0.9996(2.18)	1.002 (2.96)	1.014 (2.18)
	09-1		1.022 (3.05)	1.004 (2.90)	1.028 (2.17)		
10	10-2	4.00	1.000 (2.99)	1.007 (2.90)	1.016 (2.18)	1.024 (2.95)	1.027 (2.18)
	10-1		1.038 (2.98)	1.052 (2.93)	1.038 (2.17)		

a/ Errors quoted are ±1σ (%) from exact variance alogrithm.

b/ The average and error quoted here are unweighted means of the values obtained from the γ-ray assays.

Table 7

Comparison of Berkeley (UCB), Livermore (LLL), and Los Alamos (LASL) Measurements on Fuel Sample From Run 02.

A. UCB-LLL

E_γ(keV)	I_γ(LLL)min^{-1} [a/]	I_γ(UCB)min^{-1}	I_γ(LLL)/I_γ(UCB)	I_γ^+(LLL) [b/]	I_γ^+(UCB) [b/]
724	$(3.105\pm0.046)\times10^8$	$(3.034\pm0.050)\times10^8$	1.023±0.023	100.00	100.00
757	$(3.886\pm0.058)\times10^8$	$(3.714\pm0.061)\times10^8$	1.046±0.024	125.15±1.24	122.41±1.21
1596	$(6.480\pm0.097)\times10^7$	$(6.461\pm0.107)\times10^8$	1.003±0.023	30.87±0.21	21.29±0.21

Unweighted average = 1.024±0.023

B. UCB-LASL

Average fission rate from LASL measurement of ^{140}Ba activity by radiochemistry[c/] = 1.132×10^{12} sec^{-1}

Average fission rate from LASL measurement of ^{95}Zr decay by γ-counting[c/] = 1.137×10^{12} sec^{-1}

Average fission rate from UCB measurement of 1596 keV γ-ray from ^{140}(Ba-La)[d/] = 1.141×10^{12} sec^{-1}

Average fission rate from UCB measurement of 724 and 757 keV γ-rays from ^{95}Zr[e/] = 1.132×10^{12} sec^{-1}

a/ Corrected for decay to time of UCB assay

b/ Relative γ-ray intensities

c/ Estimated error is <3.0% (±1σ)

d/ Estimated error is 2.7% (±1σ)

e/ Estimated error is 3.27% (±1σ)

Table 8

Adopted Values for Fission Rates

Run No.	t_{irr}(hr)	$[R_f(\Delta R_f)sec^{-1}] \div 10^{12}$	ΔR_f(%)
1	1.00	1.129 ± 0.020	1.74
2	1.00	1.136 ± 0.020	1.75
12	1.00	0.9480 ± 0.0184	1.94
3	4.00	1.116 ± 0.021	1.91
4	4.00	1.107 ± 0.019	1.75
6	22.25	0.9001 ± 0.0256	2.85
8	22.25	1.015 ± 0.019	1.84
9	4.00	1.008 ± 0.019	1.84
10	4.00	1.026 ± 0.020	2.00

6. Decay Heat Results

6.1 Data Reduction Procedure

Several different data reduction schemes were tried. They are in two categories: (a) differential and (b) integral. The differential method consists of techniques to obtain the instantaneous slope of the dilatometer response curve and from it the rate of change of stored energy. The latter may be directly added to the power measured by the thermopile to obtain the decay heat power. This method could not be applied directly on a point by point basis because the data failed to display the necessary smoothness. Various least square fitting attempts were pursued. After fitting, the slopes could be determined analytically by differentiation. No generally successful procedure was found using this method for the early decay period ($t \leq 600$ sec).

In the integral approach the thermopile output is integrated to obtain the total energy transferred as a function of time after the sample arrives in the calorimeter. The results are added to the energy storage measured by the dilatometer displacement and exponential least square fitting applied to the result. The analytical expression is then differentiated to obtain the decay heat power. This method is best suited to early time.

After trying various fitting methods it was concluded that the integral method is best for the early time where the measurement depends strongly upon the dilatometer and the differential method is best for longer times where most of the decay heat is measured by the thermopile. The cooling time was divided into two periods: $t < 600$ seconds where one second scans had been used in the data records and $t > 600$ seconds where one minute scans were employed. The first step in all data reduction is to convert all the dilatometer voltage outputs to displacement using the Fotonic Sensor calibration.

Next ENDF/B-IV predicted beta power is multiplied into the factor $\frac{C}{P_o}(t)$ to obtain the displacement correction for end effects.

For the early time results ($t \leq 600$ seconds) the integral procedure is then used as follows

$$E(t)-E(t_o) \equiv \int_{t_o}^{t} P(t)dt = -C_1[\ell(t)-\ell(t_o)] + C_2 \int_{t_o}^{t} V_{th}dt$$

where t_o is the time when the sample arrives in the calorimeter. Due to a faulty adjustment in the delay sequence timer, t_o=10 seconds for Runs 1-6. For Runs 8-12 t_o=7 seconds. After exponential least square fitting of the total energy function it is differentiated to give the decay heat power.

For the longer time span ($t \geq 600$ seconds) 4th order polynomial least square fitting is applied to the corrected dilatometer displacement data and then differentiated to obtain $\frac{d\ell}{dt}$. Some noise was evident in the thermopile response so these data were smoothed. The decay heat power was then calculated from

$$P(t) = -C_1 \frac{d\ell(t)}{dt} + C_2 V_{th}(t)$$

Good agreement was obtained at the junction between the two regions. Agreement between different runs having the same irradiation time (on the basis of Mev/sec per fission/sec) is better in the long cooling time region than in the early cooling time region.

Several corrections to the basic results must be considered. They are:

- Heat leakage from the mercury vessel
- Heat source from activation of aluminum cladding
- Heat source from ^{239}U and ^{239}Np decay
- Heat source from fast fission in ^{238}U
- Gamma Leakage from the mercury absorber

The heat losses were analyzed for steady state and found to be smaller than 1% of the decay heat rate. This small effect is automatically

included in the experimentally determined constant C_2. Energy from aluminum cladding activation was calculated in the data reduction program and the correction applied. Gamma leakage was calculated by the SAM-F transport code to be on the order of ½% or less of the total decay heat. For the small dimension of our fuel samples the fast fission effect is very small and since the fissions of ^{238}U are also counted the effect on decay heat is due mainly to the difference between ^{238}U and ^{235}U fission product yields. (The decay heat from ^{238}U is a little higher). The ^{239}U and ^{239}Np contribute less than 1%. These last three effects are small and tend to compensate each other and were therefore neglected.

In order to compare results for different irradiation times all runs were converted to infinite irradiation time using

$$P(t,\infty) = P(t,T) + P(t+T,\infty) \ .$$

$P(t,T)$ is the experimental result while $P(t+T,\infty)$ is obtained from ENDF-BIV summation calculation. Thus the result is then partly theoretical and the procedure is of little value for $t \geq T$.

6.2 Decay Heat Results

Responses of the dilatometer and thermopile are shown in Figures 13 and 14 for Runs 1 and 8 respectively for the first 600 seconds of cooling time. These figures illustrate the magnitude of the "bump" at the beginning of the transient. In addition some noise is evident in both signals. These two runs represent the best data quality from the standpoint of noise.

Reduced data for 1,4 and 22.35 hr irradiation times are presented in Figures 15, 16, and 17 respectively. These data are tabulated in Tables 9-15. Each run is compared with the summation calculation result. The general trend of the data is to start higher than the theoretical result at the short cooling times. Agreement is quite good from about 500 seconds to 10^4 seconds. Then the data tend to be high again for times larger than 10^4 seconds.

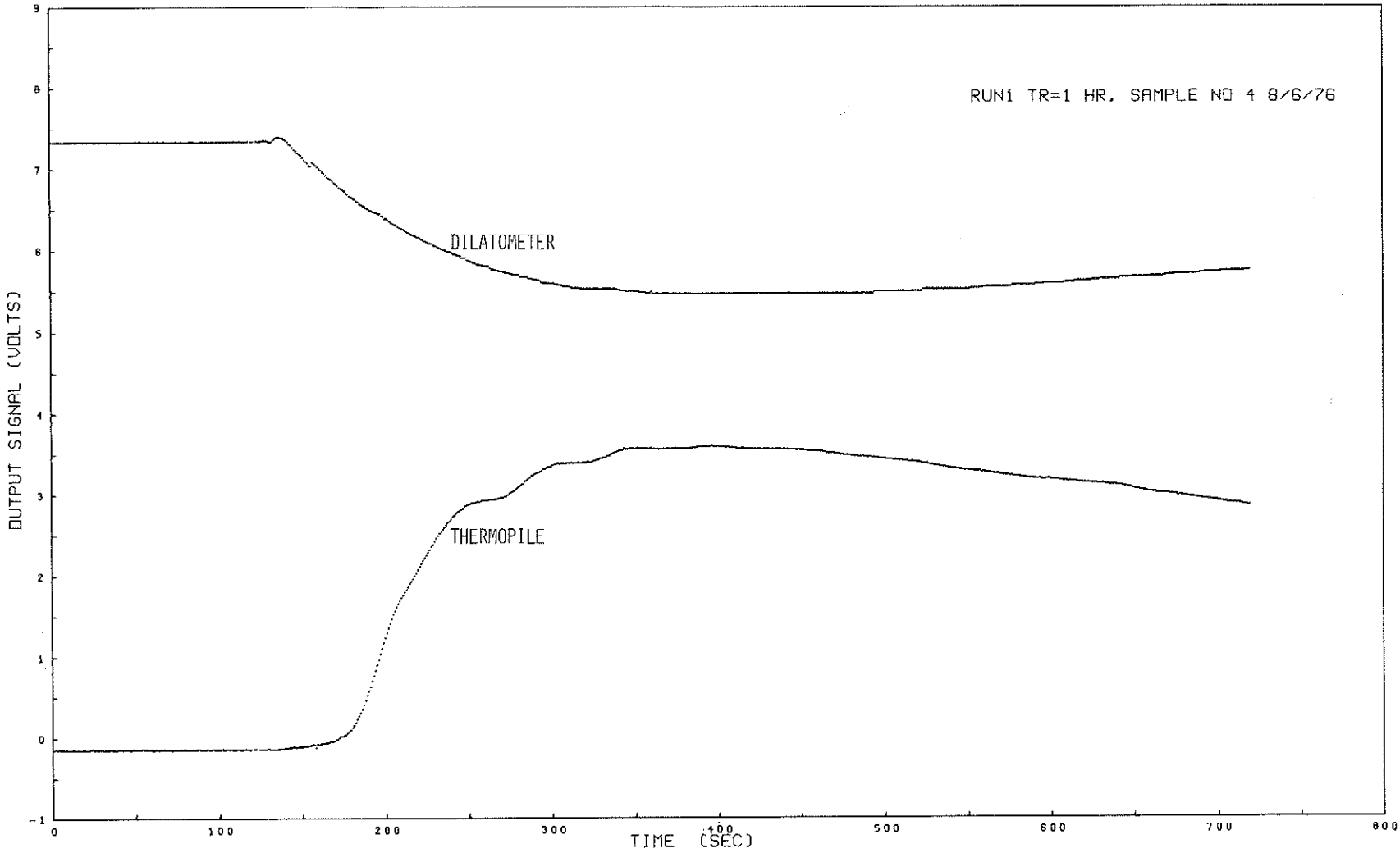

Figure 13 Raw data run 1

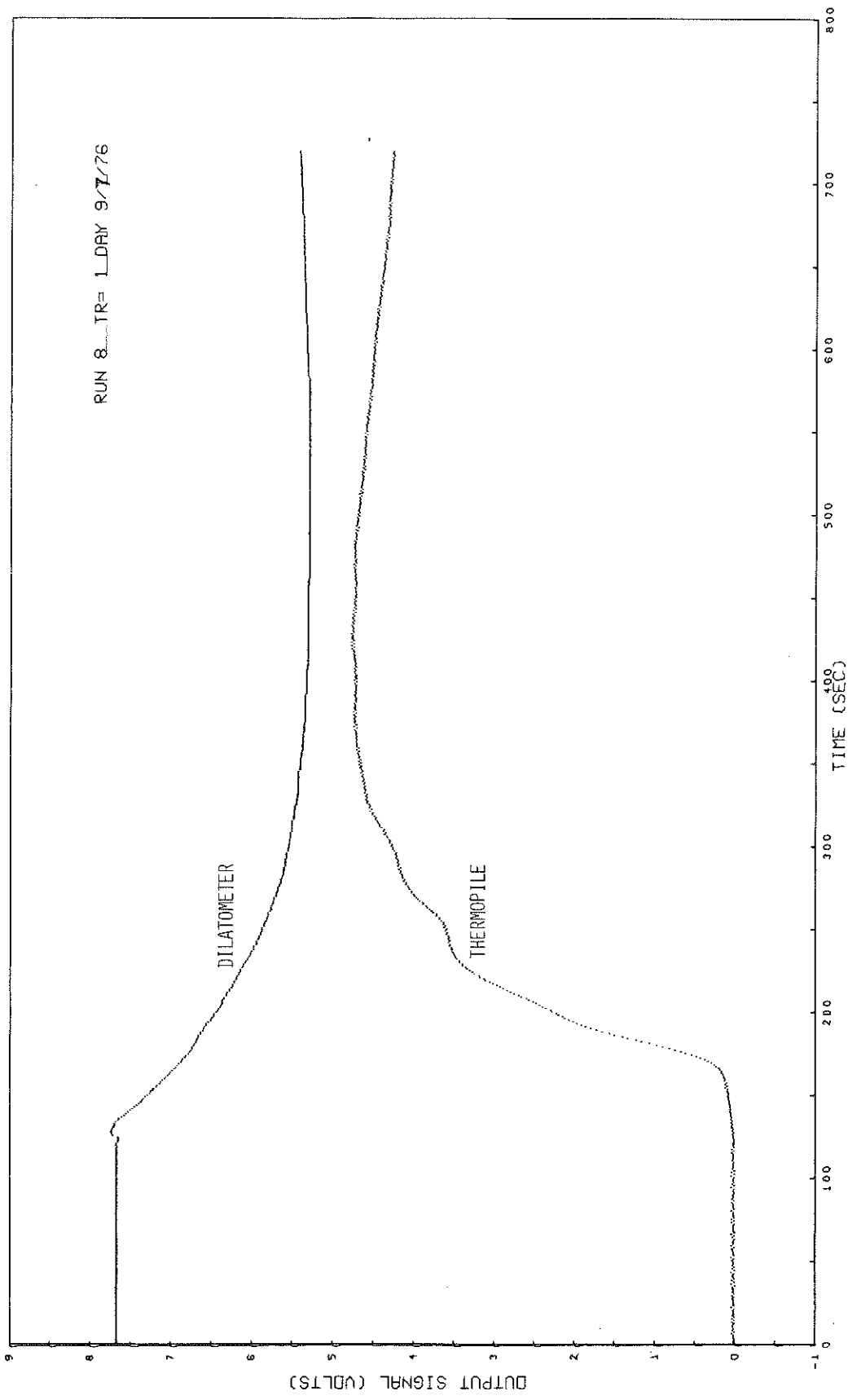

Figure 14 Raw data run 8

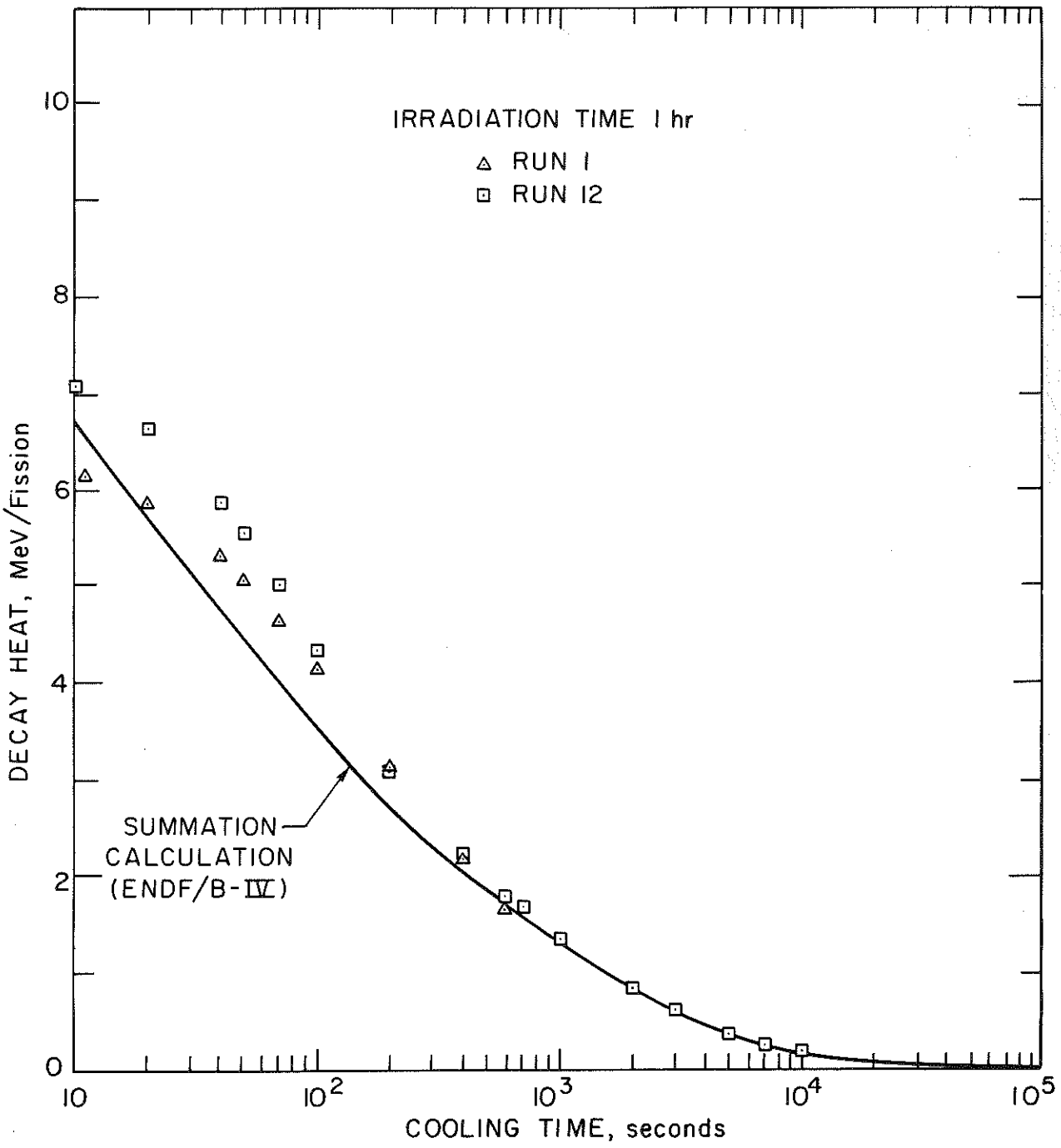

Figure 15 Decay heat results for 1 hour irradiation

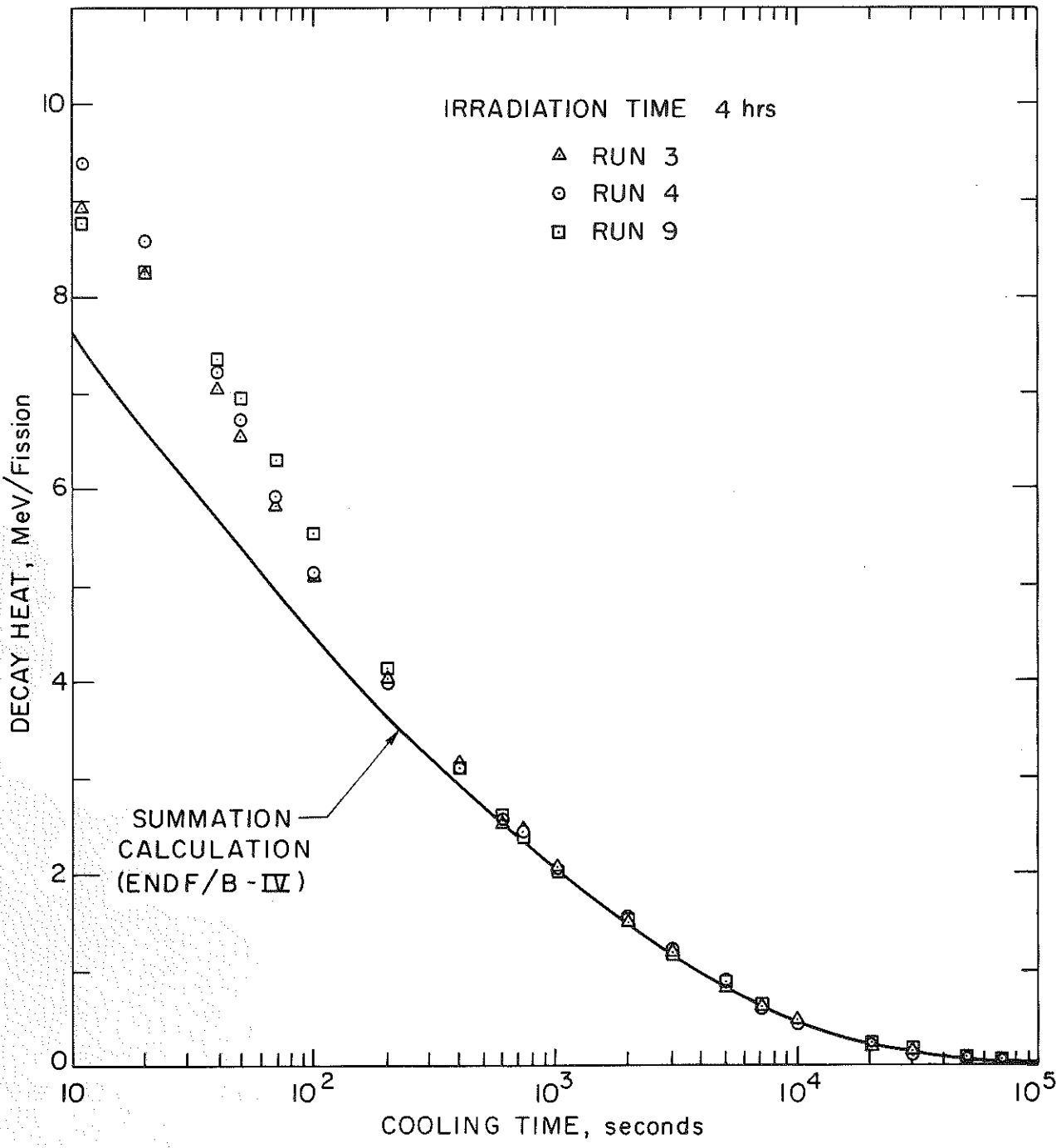

Figure 16 Decay heat results for 4 hour irradiation

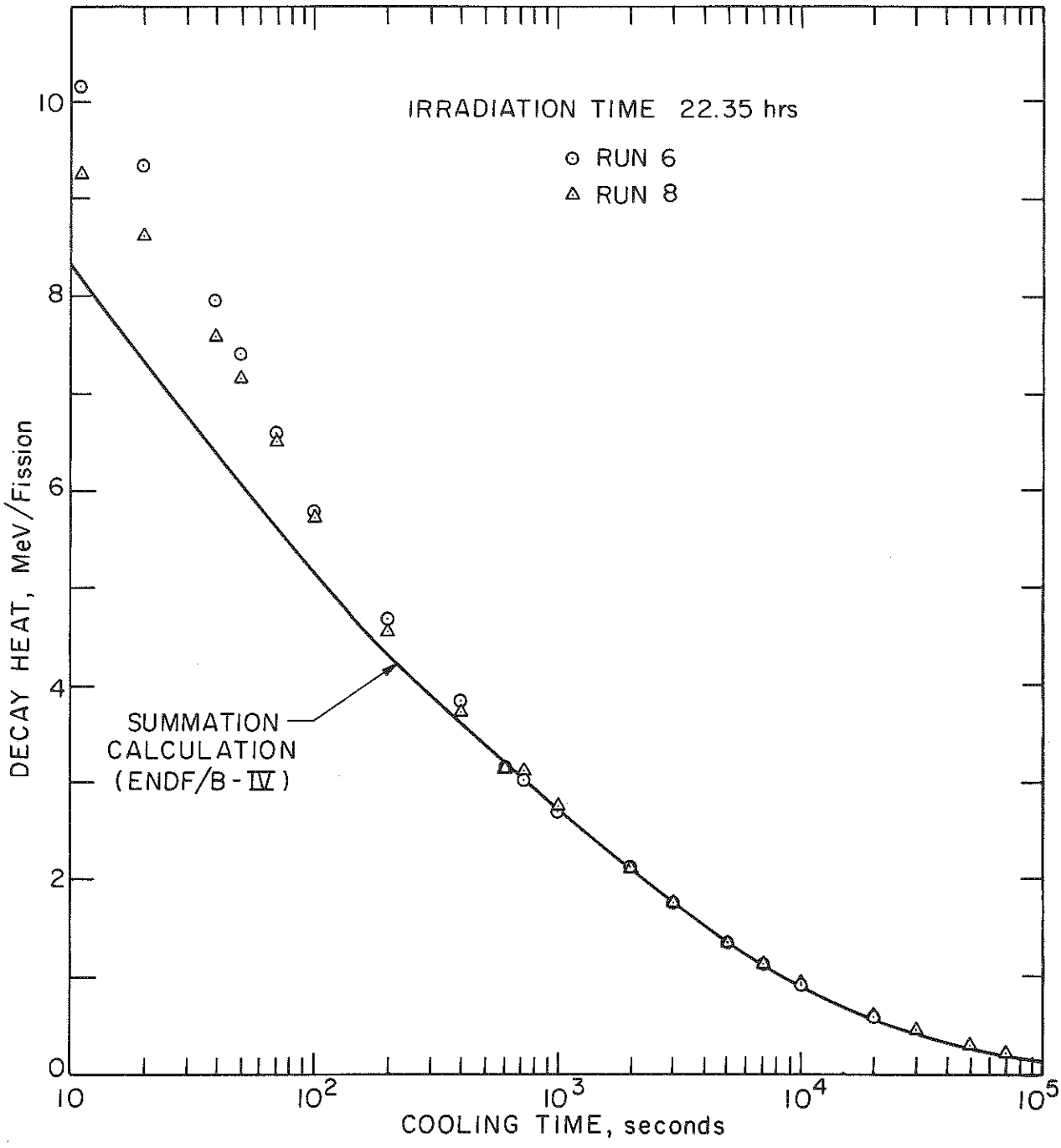

Figure 17 Decay heat results for 22.35 hour irradiation

TABLE 9

Experimental Decay Heat Power

RUN No. 1

t_r = 1 HRS.

FISSION RATE = 1.129×10^{12} fissions/sec

COOLING TIME (sec)	DECAY HEAT POWER (WATTS)	DECAY HEAT POWER $(\frac{MeV}{sec})/(\frac{Fission}{sec})$	$\frac{(DECAY\ HEAT)_{exp}^{*}}{(DECAY\ HEAT)_T}$
11	1.109	6.130	0.9344
20	1.058	5.849	1.023
40	9.592×10^{-1}	5.303	1.109
50	9.162×10^{-1}	5.065	1.128
70	8.411×10^{-1}	4.650	1.157
100	7.502×10^{-1}	4.148	1.167
200	5.636×10^{-1}	3.116	1.142
400	3.968×10^{-1}	2.194	1.060
600	3.025×10^{-1}	1.673	0.9727

* The subscript T refers to the theoretical result from summation calculations using ORIGEN, RIBD or CINDER with ENDF/B-IV Data

Table 8

Adopted Values for Fission Rates

Run No.	t_{irr}(hr)	$[R_f(\Delta R_f)sec^{-1}] \div 10^{12}$	ΔR_f(%)
1	1.00	1.129 ± 0.020	1.74
2	1.00	1.136 ± 0.020	1.75
12	1.00	0.9480 ± 0.0184	1.94
3	4.00	1.116 ± 0.021	1.91
4	4.00	1.107 ± 0.019	1.75
6	22.25	0.9001 ± 0.0256	2.85
8	22.25	1.015 ± 0.019	1.84
9	4.00	1.008 ± 0.019	1.84
10	4.00	1.026 ± 0.020	2.00

TABLE 10

Experimental Decay Heat Power

RUN No. 12

t_r = 1 HRS.

FISSION RATE = 0.9480×10^{12} fissions/sec

COOLING TIME (sec)	DECAY HEAT POWER (WATTS)	DECAY HEAT POWER $(\frac{MeV}{sec})/(\frac{Fission}{sec})$	$\frac{(DECAY\ HEAT)_{exp}}{(DECAY\ HEAT)_T}$
11	1.072	7.069	1.054
20	1.006	6.633	1.160
40	8.922×10^{-1}	5.883	1.231
50	8.435×10^{-1}	5.562	1.239
70	7.594×10^{-1}	5.008	1.246
100	6.606×10^{-1}	4.356	1.226
200	4.735×10^{-1}	3.122	1.144
400	3.384×10^{-1}	2.231	1.078
600	2.735×10^{-1}	1.803	1.048
720	2.618×10^{-1}	1.724	1.091
1020	2.077×10^{-1}	1.368	1.037
1980	1.325×10^{-1}	0.8725	1.016
3000	9.534×10^{-2}	0.6277	1.027
4980	5.926×10^{-2}	0.3902	1.034
7020	4.304×10^{-2}	0.2834	1.078
10020	3.427×10^{-2}	0.2256	1.283

TABLE 11

Experimental Decay Heat Power

RUN No. 3

t_r = 4 HRS.

FISSION RATE = 1.116×10^{12} fissions/sec

COOLING TIME (sec)	DECAY HEAT POWER (WATTS)	DECAY HEAT POWER $(\frac{MeV}{sec})/(\frac{Fission}{sec})$	$\frac{(DECAY\ HEAT)_{exp}}{(DECAY\ HEAT)_T}$
11	1.595	8.922	1.190
20	1.469	8.216	1.245
40	1.252	7.003	1.229
50	1.169	6.540	1.208
70	1.041	5.821	1.176
100	9.119×10^{-1}	5.100	1.141
200	7.195×10^{-1}	4.024	1.110
400	5.630×10^{-1}	3.149	1.071
600	4.513×10^{-1}	2.524	0.9898
720	4.424×10^{-1}	2.474	1.034
1020	3.778×10^{-1}	2.113	1.011
1980	2.682×10^{-1}	1.500	0.9870
3000	2.163×10^{-1}	1.210	1.023
4980	1.462×10^{-1}	0.8175	0.9888
7020	1.119×10^{-1}	0.6256	0.9965
10020	8.361×10^{-2}	0.4676	1.021
19980	4.066×10^{-2}	0.2741	0.9881
30000	2.639×10^{-1}	0.1476	0.9851

TABLE 12

Experimental Decay Heat Power

RUN No. 4

t_r = 4 HRS.

FISSION RATE = 1.107×10^{12} fissions/sec

COOLING TIME (sec)	DECAY HEAT POWER (WATTS)	DECAY HEAT POWER $(\frac{MeV}{sec})/(\frac{Fission}{sec})$	$\frac{(DECAY\ HEAT)_{exp}}{(DECAY\ HEAT)_T}$
11	1.662	9.372	1.249
20	1.523	8.586	1.301
40	1.283	7.237	1.270
50	1.192	6.722	1.242
70	1.051	5.925	1.197
100	9.098×10^{-1}	5.130	1.148
200	7.053×10^{-1}	3.977	1.097
400	5.508×10^{-1}	3.106	1.056
600	4.428×10^{-1}	2.497	0.9792
720	4.358×10^{-1}	2.456	1.026
1020	3.730×10^{-1}	2.103	1.006
1980	2.807×10^{-1}	1.582	1.041
3000	2.165×10^{-1}	1.220	1.031
4900	1.603×10^{-1}	0.9037	1.093
7020	1.080×10^{-1}	0.6090	0.9700
10020	7.937×10^{-2}	0.4474	0.9771
19980	4.706×10^{-2}	0.2653	1.153
30000	2.410×10^{-2}	0.1358	0.9063
49980	1.737×10^{-2}	0.09789	1.172
70020	1.448×10^{-2}	0.082	1.499

TABLE 13

Experimental Decay Heat Power

RUN No. 9

t_r = 4 HRS.

FISSION RATE = 1.008×10^{12} fissions/sec

COOLING TIME (sec)	DECAY HEAT POWER (WATTS)	DECAY HEAT POWER $(\frac{MeV}{sec})/(\frac{Fission}{sec})$	$\frac{(DECAY\ HEAT)_{exp}}{(DECAY\ HEAT)_T}$
11	1.415	8.777	1.149
20	1.329	8.247	1.250
40	1.184	7.343	1.288
50	1.122	6.959	1.285
70	1.016	6.302	1.273
100	8.927×10^{-1}	5.539	1.240
200	6.652×10^{-1}	4.127	1.138
400	5.029×10^{-1}	3.120	1.061
600	4.201×10^{-1}	2.607	1.022
720	3.829×10^{-1}	2.377	0.9931
1020	3.324×10^{-1}	2.058	0.9844
1980	2.475×10^{-1}	1.532	1.008
3000	1.924×10^{-1}	1.191	1.007
4980	1.392×10^{-1}	0.8620	1.043
7020	1.093×10^{-1}	0.6769	1.078
10020	8.038×10^{-2}	0.4977	1.087
19980	4.528×10^{-2}	0.2804	1.218
30000	3.241×10^{-2}	0.2007	1.239
49980	1.669×10^{-2}	0.1033	1.237
70020	0.7933×10^{-2}	0.0492	0.9023

TABLE 14

Experimental Decay Heat Power

RUN No. 6

t_r = 22.35 HRS.

FISSION RATE = 0.9001×10^{12} fissions/sec

COOLING TIME (sec)	DECAY HEAT POWER (WATTS)	DECAY HEAT POWER $(\frac{MeV}{sec})/(\frac{Fission}{sec})$	$\frac{(DECAY\ HEAT)_{exp}}{(DECAY\ HEAT)_T}$
11	1.470	10.19	1.243
20	1.349	9.353	1.273
40	1.144	7.933	1.240
50	1.067	7.401	1.217
70	9.501×10^{-1}	6.588	1.168
100	8.359×10^{-1}	5.796	1.129
200	6.751×10^{-1}	4.682	1.092
400	5.492×10^{-1}	3.808	1.058
600	4.560×10^{-1}	3.162	0.9850
720	4.334×10^{-1}	3.006	0.9896
1020	3.890×10^{-1}	2.697	0.9897
1980	3.073×10^{-1}	2.131	1.0016
3000	2.557×10^{-1}	1.773	1.0050
4980	1.993×10^{-1}	1.319	1.014
7020	1.658×10^{-1}	1.150	1.022
10020	1.340×10^{-1}	0.9291	1.015
19980	8.5123×10^{-2}	0.5903	1.039

TABLE 15

Experimental Decay Heat Power

RUN No. 8

t_r = 22.35 HRS.

FISSION RATE = 1.015×10^{12} fissions/sec

COOLING TIME (sec)	DECAY HEAT POWER (WATTS)	DECAY HEAT POWER $(\frac{MeV}{sec})/(\frac{Fission}{sec})$	$\frac{(DECAY\ HEAT)_{exp}}{(DECAY\ HEAT)_T}$
11	1.500	9.250	1.114
20	1.398	8.623	1.173
40	1.233	7.602	1.188
50	1.165	7.188	1.182
70	1.055	6.509	1.154
100	9.357×10^{-1}	5.771	1.25
200	7.400×10^{-1}	4.564	1.065
400	6.034×10^{-1}	3.722	1.034
600	5.178×10^{-1}	3.193	0.9947
720	5.089×10^{-1}	3.139	1.033
1020	4.452×10^{-1}	2.746	1.008
1980	3.432×10^{-1}	2.117	0.9951
3000	2.880×10^{-1}	1.777	1.007
4900	2.244×10^{-1}	1.384	1.015
7020	1.875×10^{-1}	1.156	1.028
10020	1.532×10^{-1}	0.9453	1.042
19980	9.923×10^{-2}	0.6121	1.042
30000	7.365×10^{-2}	0.4544	1.077
49980	4.902×10^{-2}	0.3024	1.125
70020	3.499×10^{-2}	0.2159	1.119

Decay heat for infinite irradiation time, calculated from the data, is presented in Table 16 and Figure 18.

6.3 Error Assessment

Error assessment based upon design features has little meaning in the final experiment. The reasons for this are

- The "end effect" i.e., the small change in mercury vessel volume due to axial thermal strain in the sample tube, required development of an appropriate correction method and it introduced a large uncertainty in the early cooling time.
- Dilatometer data were not smooth enough to permit point to point evaluation of the rate of change of displacement. The integral data reduction method was adopted for the cooling period $t \leq 600$ seconds and contrivuted to the requirement for a modified method of error assessment.
- Thermopile output was influenced by variable noise from unidentified sources at the GETR site.

In section 5 of this report the error assessment is presented in detail for the fission rate determination. As shown in Table 8, all but one run are considered to have uncertainties (one σ) in their fission rates between 1.75 and 2.00%. For the purpose of combining this contribution with others a standard value of 2.00% was adopted.

Two other contributions were considered. They are the systematic error in the calorimeter and the rms scatter of the data from different runs. Both these contributions are difficult to assess. In the case of the rms data scatter the seven good experiments used include three different irradiation times, 1 hour, 4 hours and $\sim$1 day. The fission rates differ slightly but this is of no consequence when comparing data per unit fission rate. Two methods were tried, one simply obtained the mean, $\overline{X}$, and rms deviation, s,

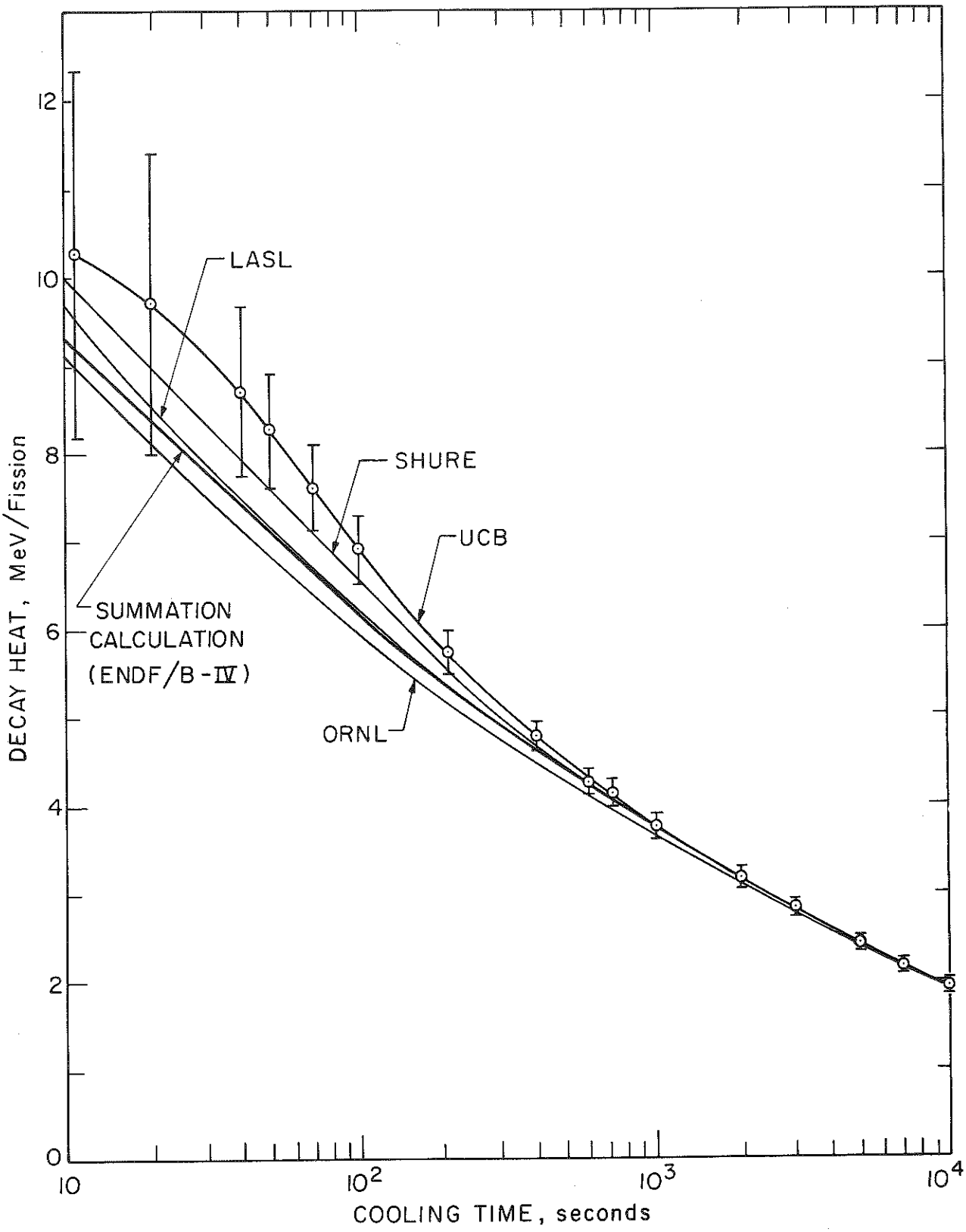

Figure 18 Comparison of UCB results with others on infinite irradiation basis

TABLE 16

DECAY HEAT POWER FOR INFINITE
THERMAL FISSION

Calculated from Experimental Data

COOLING TIME	$\overline{P}(t_c,\infty)$ mean	S	S	$\frac{P(t_c,\infty)^*}{P_o}$	$\frac{\overline{P}_{exp}}{\overline{P}_T}$
(sec)	$(\frac{MeV}{Fission})$	$(\frac{MeV}{Fission})$	%	%	
11	10.286	0.8515	8.278	5.143	1.118
20	9.710	0.6586	6.783	4.855	1.157
40	8.679	0.3642	4.196	4.340	1.170
50	8.268	0.3029	3.664	4.134	1.164
70	7.605	0.2179	2.865	3.803	1.145
100	6.894	0.1689	2.450	3.447	1.118
200	5.710	7.0242×10^{-2}	1.230	2.855	1.073
400	4.798	3.8252×10^{-2}	0.7972	2.399	1.039
600	4.231	5.4888×10^{-2}	1.297	2.116	0.9972
720	4.130	6.9465×10^{-2}	1.682	2.065	1.013
1020	3.768	3.3745×10^{-2}	0.8956	1.884	1.001
1980	3.169	3.1928×10^{-2}	1.008	1.585	1.002
3000	2.810	1.6037×10^{-2}	0.5707	1.405	1.007
4980	2.417	2.9521×10^{-2}	1.221	1.209	1.013
7020	2.159	2.2658×10^{-2}	1.049	1.080	1.008
10020	1.931	2.2989×10^{-2}	1.191	0.9655	1.008

* P_o = 200 MeV/fission

from

$$s^2 = \frac{\sum_{i=1}^{N} (x_i - \bar{x})}{N-1}$$

using the normalized decay heat results at arbitrarily selected times. In this case the influence of irradiation time is partially accounted for by the normalization of each run to the summation calculation result for the same irradiation condition. This procedure implies that mean of data so normalized should be independent of irradiation time, which is not fundamentally true. The other method used was to obtain the mean and s from infinite irradiation results calculated from the experimental data. The rms scatter results obtained by the second method are a little smaller and are considered more meaningful. They were adopted.

A time dependent systematic uncertainty was estimated from the basic data and data reduction procedure. The method involved estimating the uncertainties in power measured by the dilatometer and thermopile and then weighting them according to the power measured by each device. The dilatometer measurement error is dominated by the uncertainty in the "bump" correction. Contributions from other sources, e.g., the Fotonic Sensor calibration, were neglected. The time dependent error adopted is based on judgment and consideration of scatter of calibration data in the correction factor C(t). At cooling times $t > 600$ seconds the error in dilatometer power contributes negligibly to the error in decay heat power.

Considering the noise in the thermopile signal and the smoothing used in data reduction a conservative constant value of 0.02 W was adopted for the thermopile error.

These error estimates are combined in Table 17. They may be contrasted with the design error assessment from which it appeared that the error in measured fission rate would dominate the result giving a total uncertainty of about 3%.

TABLE 17

Evaluation of the Standard Deviation*

COOLING TIME SECONDS	DATA rms SCATTER S	CALORIMETER σ_{s_p}	FISSION MEASUREMENT σ_{s_f}	TOTAL σ
11	0.083	0.21	0.02	0.227
20	0.068	0.16	0.02	0.175
40	0.042	0.10	0.02	0.1105
50	0.037	0.06	0.02	0.073
70	0.029	0.053	0.02	0.064
100	0.025	0.047	0.02	0.057
200	0.012	0.032	0.02	0.040
400	0.008	0.026	0.02	0.034
600	0.013	0.026	0.02	0.035
720	0.017	0.026	0.02	0.034
1020	0.009	0.026	0.02	0.034
1980	0.011	0.026	0.02	0.034
3000	0.006	0.026	0.02	0.034
4980	0.012	0.026	0.02	0.034
7020	0.010	0.026	0.02	0.034
10020	0.012	0.026	0.02	0.034
30000	0.05	0.08	0.02	0.096
70000	0.10	0.18	0.02	0.21

* Expressed as a fraction of the decay heat

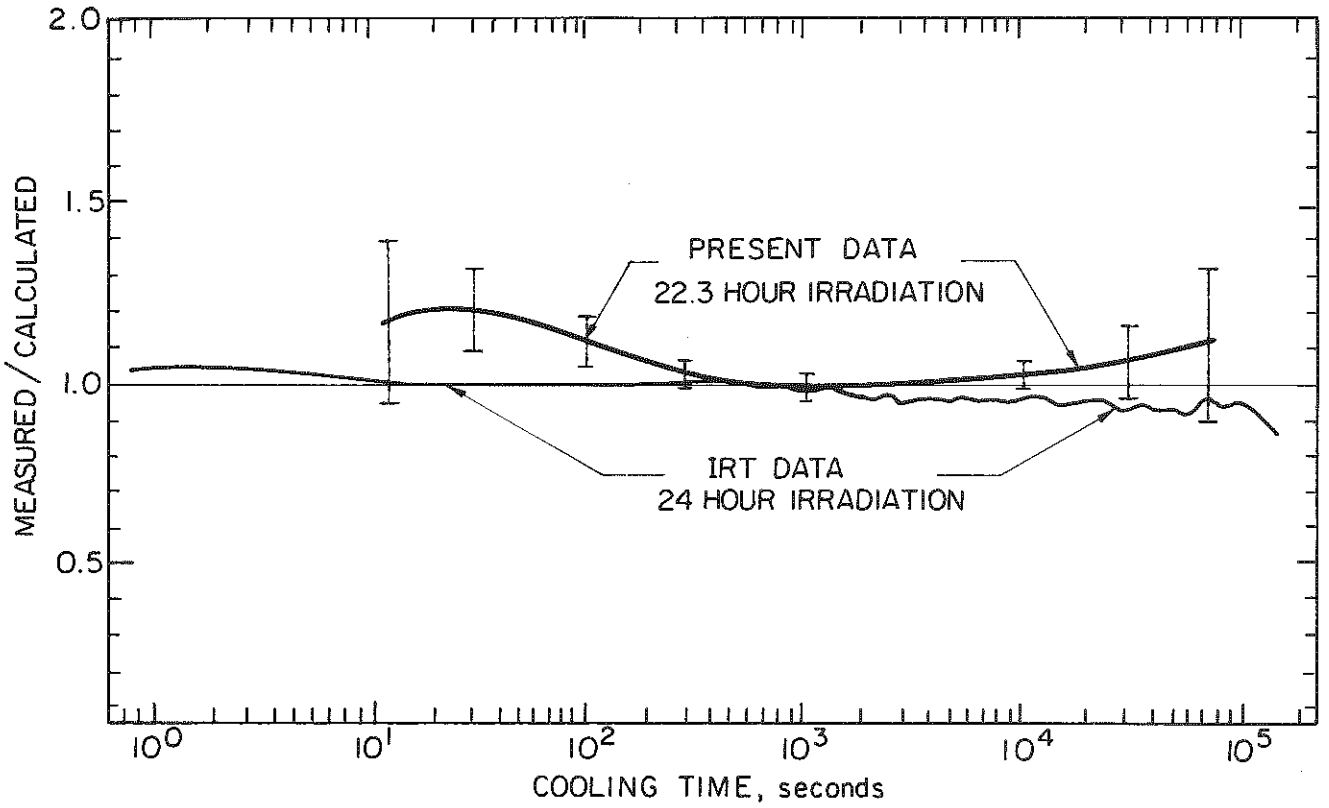

Figure 19 Comparison of UCB with IRT data for nominal 1 day irradiation

6.4 Comparison of Results with Other Experiments and Calculations

Figures 15 through 17 show the comparison of data at each irradiation time with the corresponding summation calculation result. Figure 18 shows the infinite irradiation decay heat deduced from the present data and from experiments done recently at ORNL (Dickens, et al) and LASL (Yarnell, et al). Also shown for comparison is the ENDF/B-IV data file and the curve of Shure. In Figure 19 the present results are compared to the IRT data (Friesenhahn, et al) for a nominal one day irradiation.

The present data tend to be higher than other new data, however this must be considered in the light of the large error bar at short cooling times. Between 500 and 10,000 seconds the results agree well with both the other experiments and the theoretical results. For cooling times larger than 10^4 seconds the accuracy of the present experiments deteriorates rapidly and the results are not considered significant.

7. Conclusions

a. A new approach to a fast response calorimeteric measurement of decay heat from fission products has been developed and applied. Although the results of the measurements are much less accurate than anticipated for short cooling times, the method appears to have merit and the detailed design could be improved to achieve the original accuracy goal. The problem is to eliminate the thermally induced strains that affected the volume of the mercury vessel in the present design. Additionally, more stable environmental conditions must be provided.

b. The decay heat results obtained for ^{235}U thermal fission agree well with other experiments at cooling times between 500 and 10,000 seconds. At shorter cooling times the present data are too high by up to 17% compared to the average of other data and summation calculations. No explanation for these high results have been positively identified. It is quite possible that the difference is due to systematic error associated with data correction procedures. Considering the large error bar for short cooling times the results cannot be considered in serious disagreement with the results of others.

REFERENCES

1. ANS Draft Standard, ANS 5.1, "Decay Energy Release Rates Following Shutdown of Uranium-Fueled Thermal Reactors", American Nuclear Society (1971) Revised (1973).

2. K. Shure, "Fission-Product Decay Energy", Bettis Technical Review, USAEC Report WAPD-BT-24, pp 1-17, December (1961).

3. USAEC Interim Acceptance Criteria for Emergency Core Cooling Systems (36 FR 12248 in the Code of Federal Regulations, 1971) and currently 10CRF50 Appendix K-ECCS Evaluation Models. Code of Federal Regulations, The Archives of the United States.

4. M. Lott, "Puissance Residuelle due aux Produits de Fission", Service des Experiences Critiques et de Physique des Reacteurs, Repport No. 73-83, Centre d'Etudes Nuclaires de Cadarache (1974).

5. A. M. Perry, F. C. Maienschein and D. R. Vondy, "Fission Product Afterheat--A Review of Experiments Pertinent to the Thermal Neutron Fission of ^{235}U", ORNL-TM-4197 Oak Ridge National Laboratory (1973).

6. J. K. Dickens, et al, ORNL/NUREG-14 (1977).

7. S. J. Friensenhahn, et al, "^{235}U Fission Product Decay Heat from 1 to 10^5 Seconds", Report EPRI NP-18, Electric Power Research Institute (1976).

8. M. J. Bell, "ORIGEN - The ORNL Isotope Generation and Depletion Code", ORNL-4624, Oak Ridge National Laboratory, May 1973.

9. T.R. England, "CINDER - A One Point Depletion and Fission Product Program", (Rev.), June 1964, WAPD-TM-334.

10. D.R. Marr, "A Users' Manual for Computer Code RIBD-II - A Fission Product Inventory Code", HEDL-TIME 75-26 Hanford Engineering Development Laboratory, January 1975.

11. B. Barre, "PICFEE - Programme d'integration de courbes de fissions elementaires tenant compte de l'evolution des nuclides fissiles", Note CEA.N.1203 (October 1973).

12. A. Tobias, CEGB Report RD/B/M2453 (1972) .

13. S.B. Gunst, J.C. Connor, and D.E. Conway, "Measurements and Calculations of Heavy Isotopes in Irradiated Fuels and of ^{233}U Fission-Product Poisoning," WAPD-TM-118, July 1974.

14. B.I. Spinrad, "The Sensitivity of Decay Heat to Uncertainties in Fission Yields", Nuclear Sci. & Eng. 62, 35-44 (1976).

15. F. Schmittroth, "Uncertainty Analysis of Fission-Product Decay-Heat Summation Methods", Nuc. Sci. & Eng. 59, pp 117-139 (1976).

16. F. Schmittroth and R.E. Schenter, "Uncertainties in Fission-Product Decay-Heat Calculations", Report HEDL-SA-1114 (1976).

17. K. Johnston, "A Calorimetric Determination of Fission Product Heating in Fast Reator Plutonium Fuel", Journal of Nuclear Energy, 19, 527 (1965).

18. C. Devillers, G. Lhiaubet, M. Lott, van Dat, Nyugen and F. Dufreche, "Mesure de la Puissance Residuelle des Elements Combustibles de Rapsodie - Fortissimo par Calorimetrie", Bulletin d'Information des Services Techniques, Commissariat a'lEnergie Atomique No. 181, p. 41, May 1973.

19. S.B. Gunst, D.E. Conway and J.C. Connor, "Measured and Calculated Rates of Decay Heat in Irradiated ^{235}U, ^{233}U, ^{239}Pu and ^{232}Th", N.S.E. 56, 241 (1975).

20. M. Lott, G. Lhiaubet, F. Dufreche and R. de Tourreil, "Puissance Residuelle Total Emise par les Produits de Fission Thermique de ^{235}U", Journal of Nuclear Energy, 27, 597 (1973).

21. Yarnell, et al, Report LA-NUREG-6713, "Decay Heat from Products of ^{235}U Thermal Fission by Fast Response Boil-Off Calorimetry", (1977).

22. J. Yarnell, private communication, Feb. 1977.